JGP Journal of General Physiology

ARTICLE

Role of a conserved ion-binding site tyrosine in ion selectivity of the Na^+/K^+ pump

Kerri Spontarelli[1], Daniel T. Infield[2], Hang N. Nielsen[3], Rikke Holm[3], Victoria C. Young[1], Jason D. Galpin[2], Christopher A. Ahern[2], Bente Vilsen[3], and Pablo Artigas[1]

The essential transmembrane Na^+ and K^+ gradients in animal cells are established by the Na^+/K^+ pump, a P-type ATPase that exports three Na^+ and imports two K^+ per ATP hydrolyzed. The mechanism by which the Na^+/K^+ pump distinguishes between Na^+ and K^+ at the two membrane sides is poorly understood. Crystal structures identify two sites (sites I and II) that bind Na^+ or K^+ and a third (site III) specific for Na^+. The side chain of a conserved tyrosine at site III of the catalytic α-subunit (*Xenopus*-α1 Y780) has been proposed to contribute to Na^+ binding by cation–π interaction. We substituted Y780 with natural and unnatural amino acids, expressed the mutants in *Xenopus* oocytes and COS-1 cells, and used electrophysiology and biochemistry to evaluate their function. Substitutions disrupting H-bonds impaired Na^+ interaction, while Y780Q strengthened it, likely by H-bond formation. Utilizing the non-sense suppression method previously used to incorporate unnatural derivatives in ion channels, we were able to analyze Na^+/K^+ pumps with fluorinated tyrosine or phenylalanine derivatives inserted at position 780 to diminish cation–π interaction strength. In line with the results of the analysis of mutants with natural amino acid substitutions, the results with the fluorinated derivatives indicate that Na^+–π interaction with the phenol ring at position 780 contributes minimally, if at all, to the binding of Na^+. All Y780 substitutions decreased K^+ apparent affinity, highlighting that a state-dependent H-bond network is essential for the selectivity switch at sites I and II when the pump changes conformational state.

Introduction

All vertebrate cells use the energy accumulated in Na^+ and K^+ electrochemical gradients across their plasma membranes to power essential functions, like electrical excitability or nutrient and neurotransmitter uptake. These gradients are established and maintained by the Na^+,K^+-ATPase, also known as the Na^+/K^+ pump, which is a member of the type 2C subfamily of P-type ATPases. All P-type ATPases share a similar transport cycle whereby alternating phosphorylated and dephosphorylated forms drive the conversion between two major conformations: E2 with external-facing ion-binding sites and E1 with internal-facing sites (Fig. 1 A; Sen and Post, 1964). Precise ion-selectivity mechanisms and ionic stoichiometries distinguish type 2 family members. A salient feature of the Na^+/K^+ pump is that in addition to two shared sites that can be reciprocally occupied by Na^+ or K^+ (site I and site II), there is a third site (site III) which is highly selective for Na^+ (Ratheal et al., 2010). Based on the crystal structures, the side chain of a tyrosine residue in the fifth transmembrane segment, M5 (Y780 in *Xenopus* α1, Y778 in human α1, Y773 in rat α1, and Y771 in the pig α1 from crystal structures) may stabilize the bound Na^+ at site III in one or both of the following ways: (1) through direct cation–π interaction with Na^+ (Kanai et al., 2013) and (2) through a network of hydrogen bonds that may include the side-chain hydroxyl of Y780 (Kanai et al., 2013; Nielsen et al., 2019; Fig. 1, C and D). This aromatic residue is well conserved among P-type ATPases (Fig. 1 E). The importance of this residue for ion transport is highlighted by the finding that mutation of the equivalent tyrosine in the neuron-specific α3 subunit (Y763) to cysteine or histidine causes alternating hemiplegia in childhood (AHC; Panagiotakaki et al., 2015), a debilitating neurological disorder (Holm et al., 2016). While cation–π interactions involving aromatic residues have been extensively studied in ion channels in relation to ion pore function and inhibitor binding (Infield et al., 2021; Roux, 2005), the putative roles of aromatic residues in ion binding to ion pumps remain largely suggestive. Previous studies evaluating the effect of Y780 mutation on Na^+/K^+ pump function are somewhat contradictory: Arguello et al. (1999) concluded that mutations Y780A, Y780S, and Y780F affected Na^+ interaction,

[1]Department of Cell Physiology and Molecular Biophysics, Center for Membrane Protein Research, Texas Tech University Health Sciences Center, Lubbock, TX; [2]Department of Molecular Physiology and Biophysics, University of Iowa, Iowa City, IA; [3]Department of Biomedicine, Aarhus University, Aarhus C, Denmark.

Correspondence to Pablo Artigas: pablo.artigas@ttuhsc.edu; Bente Vilsen: bv@biomed.au.dk.

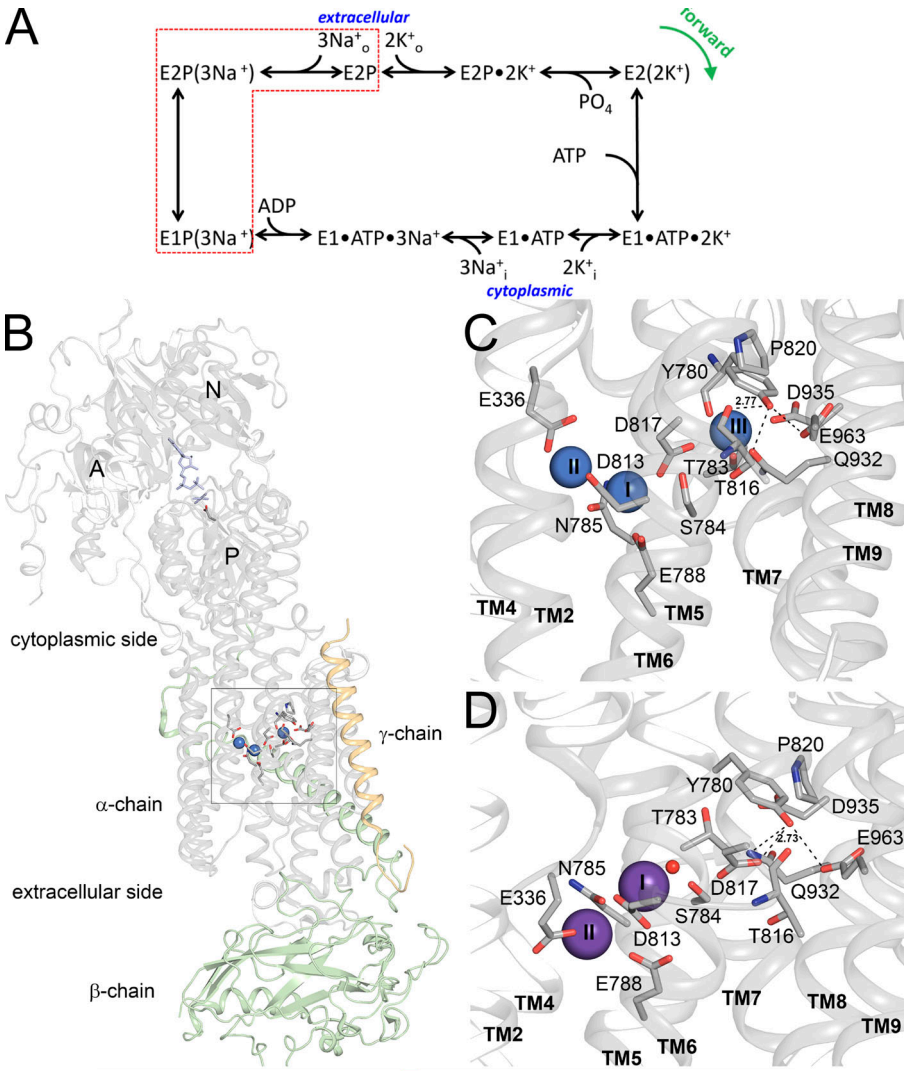

E

P2-NKA	(775)	KKSIAYTLTSNIPEITPFLIFIIANIPL
P2-HKA	(784)	KKSIAYTLTKNIPELTPYLIYITVSVPL
P2-SERCA	(758)	KQFIRYLISSNVGEVVCIFLTAALGLPE
P2-PMCA	(853)	SKFLQFQLTVNVVAVIVAFTGACITQDS
P1-ATPase	(918)	DRFSGYFVPFIIIMSTLTLVVWIVIGFI
P3-ATPase	(644)	KNYTIYAVSITIRIVFGFMLIALIWKFD
P4-ATPase	(841)	SKCILYCFYKNIVLYIIEIWFAFVNGFS

Figure 1. **Relevant functional and structural properties of the Na^+/K^+ pump. (A)** Post-Albers kinetic scheme describing partial reactions in the Na^+/K^+ pump cycle. **(B)** Overall view of the Na^+/K^+ pump structure in E1($3Na^+$) form, PDB accession no. 3WGV. The boxed part shows the ion-binding region (with three Na^+ ions as blue spheres; see further below). In the cytoplasmic region, the nucleotide, phosphate analog (both in blue stick representation) and phosphorylated aspartate (stick representation in color by elements) are shown. **(C)** Zoomed-in view of the ion-binding region of the E1($3Na^+$) structure showing amino-acid side chains participating in ion coordination, as well as Y780 and surrounding residues (stick representation in color by elements). Broken lines indicate potential hydrogen bonds from Y780 (2.77 indicates the length in A of the bond between Y780 hydroxyl and T816 backbone oxygen). Numbers on the Na^+-ions (blue spheres) are the ion-binding site number. **(D)** Zoomed-in view of the ion binding region of E2P_i($2K^+$) structure (PDB accession no. 2ZXE) with the same residues shown. K^+ ions and a water molecule are shown as purple spheres and a red sphere, respectively. Broken lines indicate potential hydrogen bonds from Y780 (2.73 indicates the length in A of the bond between Y780 hydroxyl and D817 side-chain oxygen). Note that Y780 exchanges its hydrogen-bonding partner from T816 to D817 in connection with the E1–E2 conformational change (in E2 the length between Y780 hydroxyl and T816 backbone oxygen has increased to 4.95 A). **(E)** Amino-acid sequence alignment of the catalytic subunit of P-type-ATPases showing high conservation of the tyrosine residue studied in this article. P2-ATPaseses shown are Na^+,K^+-ATPase α1 subunit (NKA), the gastric H^+,K^+-ATPase α subunit (HKA), the plasma membrane Ca^{2+}-ATPase catalytic subunit (PMCA), and the sarcoplasmic/endoplasmic reticulum Ca^{2+}-ATPase catalytic subunit (SERCA). Other P-type ATPases indicated are the Cu-ATPase ATP7B (P1-ATPase), the H^+-ATPase from *Arabidopsis thaliana* (P3-ATPase), and the human flippase ATP8A1 (P4-ATPase).

without effect on K^+ interaction, while Pedersen et al. (1998) reported that any modification of the Y780 side chain reduced the interaction of the Na^+/K^+ pump with both transported ions. However, neither article provided a clear picture of the interactions that make this residue so critical for transport, and electrophysiological studies, allowing distinction between interactions with intra- and extracellular ions, were not applied.

Here, we use electrophysiology and biochemistry to evaluate the functional effects of substituting the tyrosine at position 780 with several natural and unnatural amino acids. The results demonstrate that (1) substitutions disrupting the hydrogen bonds at Y780 impaired interaction with internal and external Na^+ while Y780Q strengthened it, (2) all Y780 substitutions reduced apparent affinity for external K^+, reinforcing the notion that a hydrogen bond network, which changes during the E1–E2 conformational transition, is essential for the alteration of selectivity between the Na^+-binding and K^+-binding forms of the Na^+/K^+ pump, (3) a cation–π interaction is unlikely to play a major role in Na^+ binding, although such interaction is suggested by the structural position of Y780 in relation to Na^+ in site III, and (4) the methods used to perform atomic mutagenesis with ion channels can be successfully applied to active transporters with transport rates >10^4 slower than those in channels.

Materials and methods

Molecular biology

Point mutations were introduced into full-length cDNA encoding the ouabain-resistant α1 subunits (the *Xenopus* Q120R/N131D-α1 or rat α1-isoform of Na^+,K^+-ATPase) using PCR, and verified by sequencing (Holm et al., 2017; Nielsen et al., 2019), both before oocyte injection or transfection into COS-1 cells

using the Ca^{2+}-phosphate precipitation method (Chen and Okayama, 1987) and after expanding single colonies into stable cell lines under ouabain selection pressure (Holm et al., 2015; Holm et al., 2017; Nielsen et al., 2019). For simplicity, throughout the manuscript, we use *Xenopus* α1 numbering (seven higher than rat α1 and nine higher than the pig α1 from crystal structures).

Oocyte preparation and electrophysiology

Oocytes were extracted from female *Xenopus laevis* toads and enzymatically dissociated as described (Meyer et al., 2017). Upon dissociation, oocytes were kept in SOS solution composed of (in mM) 100 NaCl, 1 $MgCl_2$, 2 KCl, 1.8 $CaCl_2$, 5 HEPES, 2.5 pyruvic acid (Sigma-Aldrich), 1× antibiotic-antimycotic (Gibco), and 5% horse serum (Gibco), titrated to pH 7.5 with NaOH. Oocytes were injected with cRNA mixtures of *Xenopus* Q120R/N131D-α1:β1 (75 ng α1, 25 ng β3). When using non-sense suppression, 25 µg pellets of pyrrolysine tRNA loaded with the indicated amino acid were resuspended in cold 3 mM pH 5 NaOAc and added to the mixture of cRNA (10 µg tRNA, 2 µg cRNA). A total of 50 nl of the RNA mixture was injected into each oocyte on the first day, and then 50 nl of tRNA alone was injected on subsequent days until the day of recording. Oocytes were kept at 16°C until recording (3–5 d).

Two-electrode voltage clamp (TEVC) was performed using an OC-725C amplifier (Warner Instruments) controlled by pClamp software through a Digidata 1440 (both from Molecular Devices) and were utilized for data acquisition at 10 kHz. Data were also continuously recorded with a Minidigi 1A at 1 kHz. Glass microelectrodes resistance was 0.2–1 MΩ when filled with 3 M KCl.

To increase the intracellular Na^+ concentration, a rate-limiting factor for maximal Na^+/K^+ pump cycling (Meyer et al., 2017), oocytes were incubated for 1 h in a Na^+-loading solution containing (in mM) 90 NaOH, 20 TEA-OH, 40 HEPES, and 0.2 EGTA (which chelates Ca^{2+}, causing connexin channels to open and allowing Na^+ to follow its concentration gradient), titrated to pH 7.2 with sulfamic acid (~220 mOsm/kg), and then kept in the Na^+ external solution until recording.

The recording solutions contained (in mM) 133 methanesulfonic acid (MS), 5 $Ba(OH)_2$, 1 $Mg(OH)_2$, 0.5 $Ca(OH)_2$, 10 HEPES, and 125 of either NaOH (Na^+ solution) or *N*-methyl *D*-glucamine ($NMDG^+$ solution), and were titrated to pH 7.6 with MS (250–260 mOsm/kg). K^+ was added from a 450 mM K-MS stock solution. Ouabain (10 mM) was dissolved directly in external solutions. There were no outward currents in the absence of added K^+ in $NMDG^+$ solution, indicating that the contamination of K^+ of the $NMDG^+$ used in this study (66930; Sigma-Aldrich) is negligible. When K^+ dose-response curves required concentrations above 10 mM, ouabain sensitive K^+-induced currents were used (Y780Q and Y780A).

Patch-clamp was performed essentially as described (Meyer et al., 2020; Stanley et al., 2016). The pipette solution was $NMDG^+$ external solution with 5 mM K^+ and 1 µM ouabain to inhibit endogenous pumps. The bath intracellular solution was composed of (in mM) 110 glutamic acid, 10 TEA-Cl, 10 HEPES, 5 EGTA, and 1 $MgCl_2$, with either 125 $NMDG^+$ or 125 NaOH (pH 7.4, 250–260 mOsm/kg). Intermediate Na^+ concentrations were achieved by mixing $NMDG^+$ and Na^+ intracellular solutions. MgATP was added from 200 mM stocks (pH 7.4 with $NMDG^+$). All electrophysiological experiments were performed at room temperature (22–23°C).

Biochemical analyses

Like the WT, the mutants Y780F/L/Q/A were all able to support the growth of the COS-1 cells in the presence of ouabain to inhibit the endogenous Na^+/K^+ pump, thus indicating that the mutants were able to actively transport ions. Na^+,K^+-ATPase activity, and phosphorylation with [γ-^{32}P]ATP were determined as previously described (Holm et al., 2015; Nielsen et al., 2019) under the conditions stated in the relevant figure legends, on the plasma membrane fraction from the cells. Plasma membranes were isolated by differential centrifugation and made leaky with alamethicin to allow the access of ligands from both sides of the membrane. The ATPase activity was measured by Pi liberation using the colorimetric procedure of Baginski et al. (1967) for 15–19 min. The phosphorylation and dephosphorylation reactions were performed under stirring and were quenched with ice-cold 1 M phosphoric acid, pH 2.4. The acid-precipitated ^{32}P-labeled phosphoenzyme was washed by centrifugation and quantified by phosphorimaging using a cyclone storage system (PerkinElmer Life Sciences; Nielsen et al., 2019).

Synthesis of PYL-tRNA loaded with unnatural amino acids

General information

All solvents and reagents were supplied by Sigma-Aldrich and were used as-is unless explicitly stated, and 5′-*O*-phosphoryl-2′-deoxycytidylyl-(3′→5′) adenosine (pdCpA) was obtained through GE Healthcare/Dharmacon. All *N*-Boc–protected amino acids were supplied by ChemImpex International, except for *N*-Boc-3-fluoro-*L*-tyrosine (1ClickChemistry, Inc.) and *N*-Boc-*L*-Cho cyanomethyl ester (AsisChem, Inc.). Dry nitrogen was supplied by Praxair and passed through two moisture scrubbing columns of dry calcium sulfate (Drierite) prior to use. HPLC analyses were performed on a Waters 1525 Binary HPLC pump equipped with a Waters 2998 Photodiode Array Detector, employing Sunfire C18 analytical (3.5 µm, 4.6 mm × 150 mm, 0.8 ml/min) or preparative (5.0 µm, 19 mm × 150 mm, 10 ml/min) columns and Empower software; buffers were drawn in linear gradients from 100% A (50 mM ammonium acetate) to 100% B (acetonitrile) over 30 min. UV–visible spectra for concentration determinations were recorded on a Thermo Fisher Scientific Nanodrop 2000C spectrophotometer. Mass spectra were recorded on a Waters QToF Premier Quadrupole instrument, in both positive and negative modes.

Cyanomethyl ester of Boc-protected amino acids

The cyanomethyl esters of Boc-protected amino acids were prepared and purified as in Robertson et al. (1991). The 4-hydroxycyclohexyl amino acid (Cho) was purchased as a Boc/cyanomethyl ester compound.

Synthesis of acyl dinucleotides of L-Phe, 4-fluoro-L-Phe, 3,5-difluoro-L-Phe, L-Tyr, 3-fluoro-L-Tyr, β-cyclohexyl-L-alanine (Cha), β-(4-hydroxy) cyclohexyl-L-alanine (Cho)

Slight modifications from the published procedure were employed (Hohsaka et al., 1999; Robertson et al., 1991). A

representative synthesis is described here for Phe. The cyanomethyl ester of Boc-*L*-phenylalanine (0.04 mmol) and pdCpA (5 mg, 0.008 mmol) was dissolved in dry dimethylformamide (200 µl) in a screw-top vial (1 dram) and tetrabutylammonium acetate (30 mg, 0.1 mmol) was added. The solution was stoppered and stirred at room temperature and monitored by HPLC over several hours (2 µl aliquots were removed and diluted into 100 µl of a 4:1 mixture of A:B buffer prior to injection) with detection at 261 nm. Unreacted pdCpA elutes at ∼9 min and the Boc-*L*-phenylalanine pdCpA product around 10–13 min. The entire reaction was chromatographed on a Waters 1525 Binary HPLC pump equipped with a Waters 2998 Photodiode Array Detector, employing a Sunfire preparative (5.0 µm, 19 × 150 mm, 10 ml/min) C18 column. Buffers were drawn in a linear gradient from 100% A (50 mM ammonium acetate) to 100% B (acetonitrile) over 30 min. The product peak was isolated, frozen, and lyophilized. The residue was treated with ice-cold trifluoroacetic acid (∼300 µl) placed on an ice bath for 30 min to facilitate the removal of the Boc group. Excess trifluoroacetic acid was removed in a gentle stream of dry nitrogen gas until a sticky oil remained and ice-cold ether was added to precipitate the TFA salt of *L*-Phe-pdCpA, which was washed twice more with ether and very carefully dried in a gentle stream of dry nitrogen gas. The resulting granular powder was stored as a salt at −20°C. Mass spectrometry confirmed the identity of the molecule (Fig. 2). When needed for ligation to full-length tRNA this material was carefully dissolved in ∼50 µl dry DMSO and checked for product integrity via HPLC, and stock concentration was approximated on a NanoDrop UV-vis spectrometer using the known molecular extinction coefficient for pdCpA. *L*-Phe-pdCpA isolated in this manner had its concentration adjusted to 3 mM with DMSO and the stock was stored in aliquots at −28°C.

Ligation of tRNA

An amber suppressor pyrrolysine (*PylT*) tRNA lacking the last two nucleotides (-CA; Infield et al., 2018) was generated either by in vitro transcription, using the method described previously in detail (Leisle et al., 2016) or synthesized and HPLC purified by Integrated DNA Technologies. Pellets of tRNA were resuspended in 10 mM HEPES, pH 7.4, and refolded by heating to 94°C for 3 min followed by linear cooling in a thermocycler to 4°C over 20 min. For each ligation, 25 µg (in 30 µl volume) of refolded tRNA was added to 28 µl of DEPC-treated water, 8 µl of ∼3 mM DMSO stocks of pdCpA with or without appended amino acid, 1 µl of ATP (10 mM stock, New England Biolabs [NEB]), 5 µl of T4 RNA ligase 1 (NEB) and 8 ml of T4 RNA ligase buffer (NEB). This 80 µl ligation reaction was incubated for 2 h at 4°C. The acylated tRNA was purified via phenol–chloroform extraction and ethanol precipitation. The tRNA pellets were washed in 70% ethanol, dried via Speedvac, and stored at −80°C or on dry ice until used for injection.

Data analysis and statistics

Data points shown in the figures are mean and error bars are SEM, while data in the main text and table are mean ± SD. The SigmaPlot program (SPSS, Inc.) or Origin (Originlab Corp) were used to fit relevant equations to data points using non-linear regression. The ligand concentration dependencies of the distinct enzymatic reactions and currents were fitted by a Hill function (Eq. 1):

$$A = A_0 + A_{max}\left(\frac{[L]^n}{K_{0.5}^n + [L]^n}\right), \quad (1)$$

where A_0 is the activity or current in the absence of the ligand, A_{max} is the maximum value reached at infinite ligand concentration, $K_{0.5}$ is the ligand concentration giving half-maximal activation (1/apparent affinity), and n is the Hill coefficient.

The K^+ dependence of phosphorylation was fitted by representing the inhibitory ligand (i.e., K^+) binding by a negative Hill function (Eq. 2):

$$A = A_0 + A_{max}\left(1 - \frac{[L]^n}{K_{0.5}^n + [L]^n}\right). \quad (2)$$

A_{max} is the maximum value of the variable fraction corresponding to zero concentration of the inhibitory ligand. A_0 is the phosphorylation corresponding to infinite ligand concentration, i.e., maximal inhibition.

Likewise, for K^+ dependence of ATPase activity, in the cases where inhibition was observed at high K^+ concentrations, a negative Hill function representing the inhibition was added to the Hill function in Eq. 1.

The determination of the E1P–E2P distribution of the phosphoenzyme was based on fitting a double exponential decay function to the dephosphorylation time course (Eq. 3):

$$EP = E_1 Pexp^{(-k_1 t)} + E_2 Pexp^{(-k_2 t)}. \quad (3)$$

EP is the total amount of phosphoenzyme. E1P and E2P are the two phosphoenzyme intermediates that are ADP- and K^+-sensitive, respectively. Here, k_1 and k_2 are the decay constants for the E1P and E2P phases, respectively.

Transient currents elicited after a 50- or 100-ms-long pulse were baseline-corrected with a time-independent constant and integrated. The Q–V curves were fitted with a Boltzmann distribution (Eq. 4):

$$Q_{OFF} = Q_{hyp} + \frac{Q_{tot}}{1 + \exp\left(\frac{z_q e(V - V_{1/2})}{kT}\right)}. \quad (4)$$

Q_{hyp} is the charge moved by hyperpolarizing pulses, Q_{tot} is the total charge moved, $V_{1/2}$ is the center of the distribution, z_q is the valence of a charged particle if it crossed the entire membrane electric field, e is the elementary charge, k is the Boltzmann constant, and T is the temperature. $kT/z_q e$ relates to the steepness of the curve and is also called the slope factor.

Results

We began to study the contribution of tyrosine 780 to ion binding by introducing the conservative aromatic substitution, Y780F. The mutant was expressed in *Xenopus* oocytes to perform a functional evaluation with TEVC and patch clamp, as well as in COS-1 cells to evaluate the enzymatic reactions (Figs. 3 and 4).

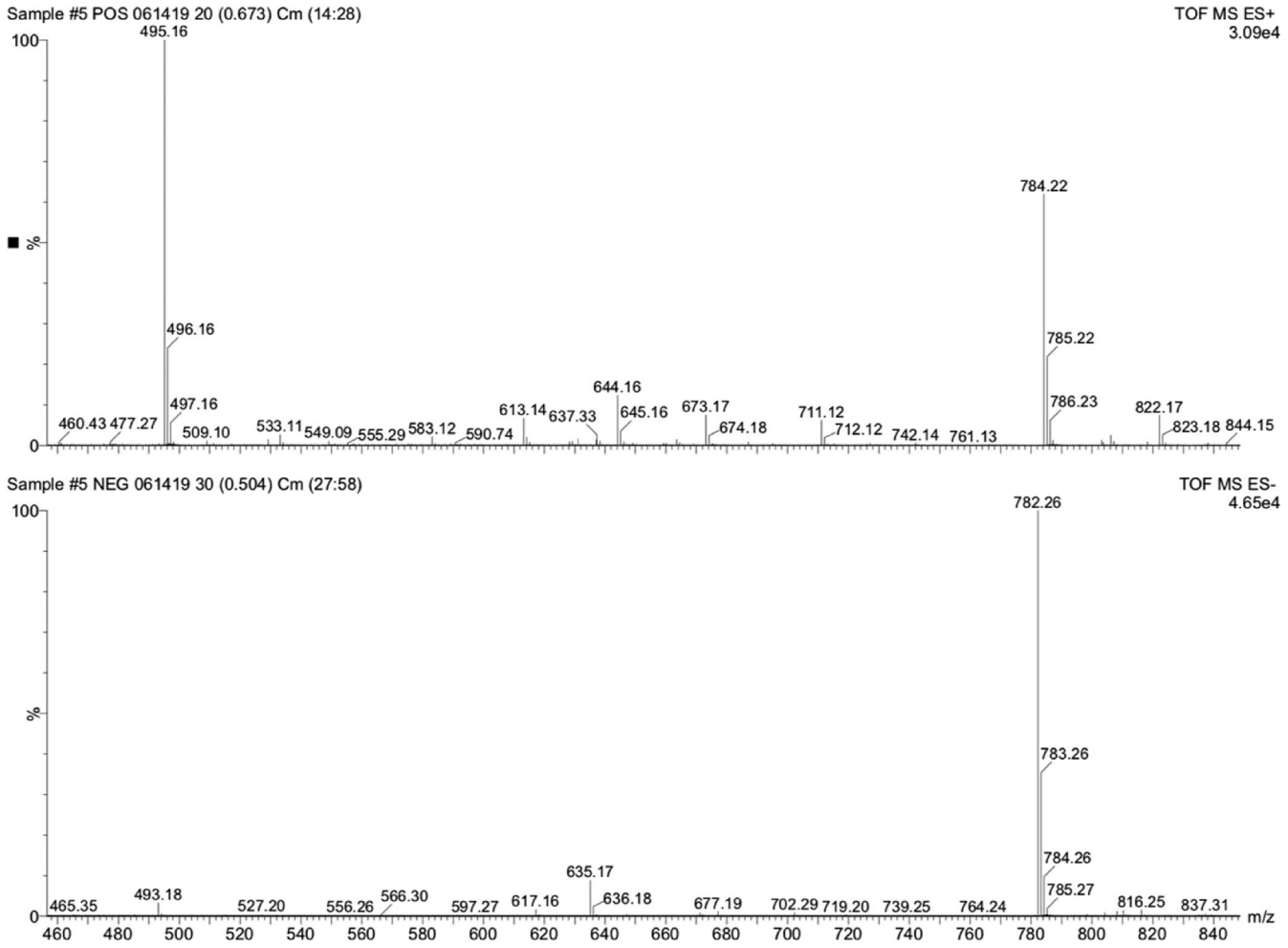

Figure 2. **Representative LRMS (± mode) of Phe-pdCpA.** Calculated mass for $C_{28}H_{35}N_9O_{14}P_2$, 783.18 D.

Representative traces at −50 mV from Na^+-loaded oocytes expressing WT or Y780F illustrate activation of outward current due to the extrusion of one charge per cycle when the indicated K^+ concentrations are applied in an external solution, where $NMDG^+$ substitutes extracellular Na^+ (Fig. 3 A). From the K^+-concentration dependence of outward current, we obtained the maximal pump current (Fig. 3 B), as well as the half-maximal activating concentration ($K_{0.5,K}$). In the absence of external Na^+, the true affinity ($1/K_{0.5}$) for externally facing sites is estimated as the E2P state accumulates. The bar graph in Fig. 3 C compares the $K_{0.5,K}$ obtained at −50 mV in $NMDG^+$ (conditions like in Fig. 3 A) and the presence of 125 mM Na^+ to illustrate the effect of external Na^+/K^+ competition. In the absence of Na^+, removal of the hydroxyl group causes a 6.4-fold reduction in apparent affinity for external K^+. A much less dramatic effect (1.5-fold reduction) was observed in the presence of Na^+, suggesting that there is a reduction in the affinity for both K^+ and Na^+, but a larger reduction in Na^+ affinity than in K^+ affinity.

To evaluate the effect of Y780F on the apparent affinity for external Na^+ in the absence of K^+, we measured the transient charge movement generated when the Na^+/K^+ pumps transit between the Na^+-bound E1($3Na^+$) and the Na^+-free E2P (Meyer et al., 2020; Moreno et al., 2020; Fig. 3, D–H). Square voltage pulses (500-ms long, illustrated within the box) were first applied in the absence of ouabain and then in its presence, and the current in the presence of ouabain was subtracted from the current in its absence, yielding the Na^+/K^+ pump-mediated transient current. The representative traces in Fig. 3, D and E, show these currents for a WT- and a Y780F-expressing oocyte, respectively. The top traces were obtained at 125 mM and the bottom ones at 62.5 mM Na^+. Because the effect of negative voltages is to promote rebinding of external Na^+, a reduction in Na^+ concentration requires more negative voltages to cause such rebinding. This correlates to a shift in the Q–V curves (Fig. 3, F–H) obtained by integrating the current traces.

As the equilibrium at −50 mV is disrupted when the pulse is turned on, the charge measured at the applied voltages (Q_{ON}) should be equal to and of opposite sign relative to the charge observed when the voltage returns to holding potential, as seen in the Q–V curves of Fig. 3, G and F. However, due to a small but obvious inward current at negative voltages (which is switched off at the same rate as the transient current is moved), Q_{ON} is frequently larger than Q_{OFF} at very negative potentials, and this difference is altered by mutations affecting Na^+ affinity (Meier et al., 2010; Nielsen et al., 2019; Yaragatupalli et al., 2009). Hence, for the rest of this article, we will limit our analysis to

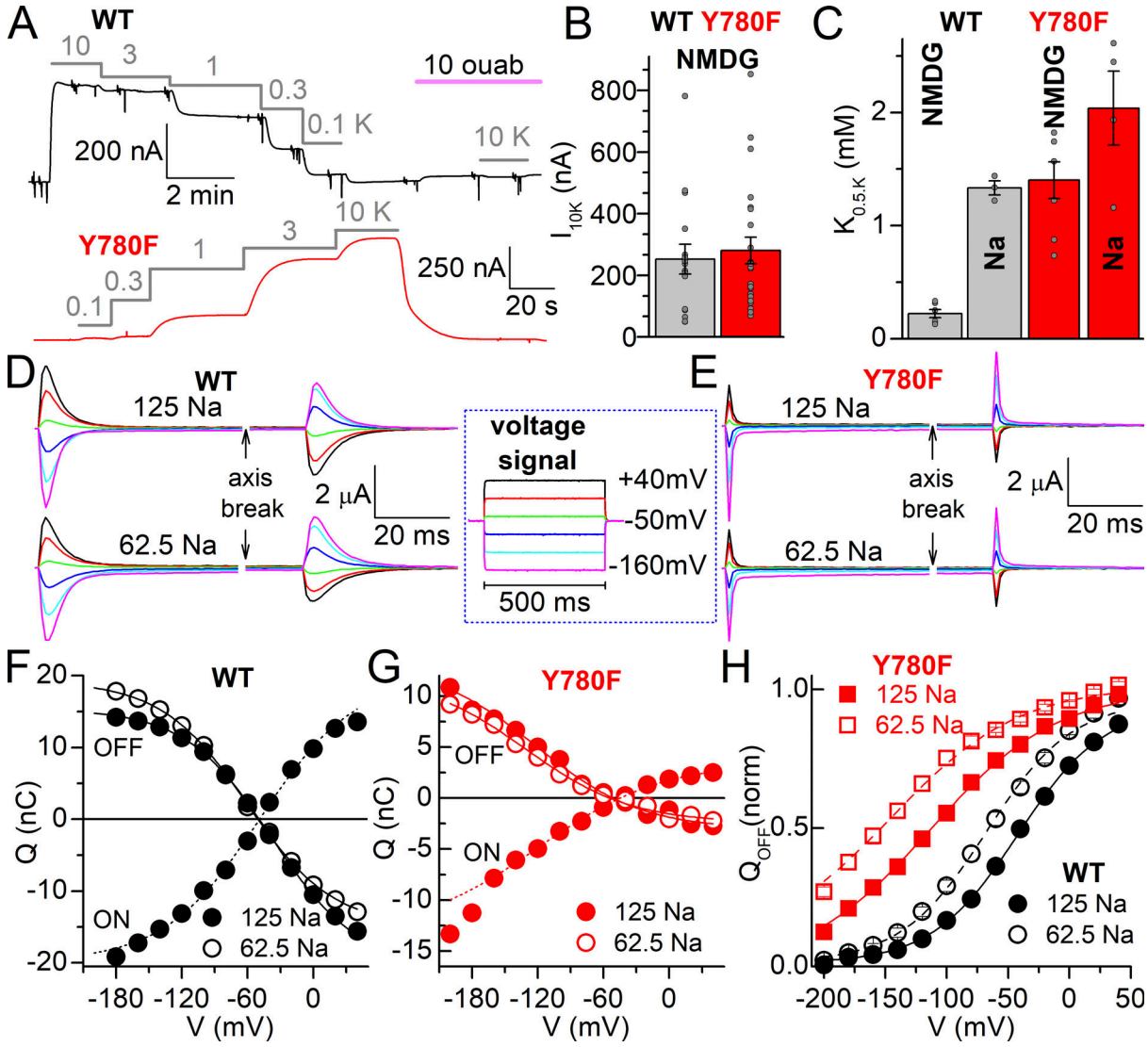

Figure 3. **Interaction with extracellular ions of WT and Y780F. (A)** Representative currents at −50 mV from oocytes expressing WT and Y780F mutant. Application of K^+ in $NMDG^+$ external solution at the millimolar concentrations indicated over the grey lines activates Na^+/K^+ pump current. At −50 mV all current induced by ≤10 mM K^+ is Na^+/K^+ pump current (Meyer et al., 2020; Stanley et al., 2015). **(B)** Pump current amplitude induced by 10 mM K^+ in $NMDG^+$, number of oocytes indicated in parentheses. **(C)** $K_{0.5.K}$ from Hill plots of dose-response data in $NMDG^+$ and in 125 mM Na^+. Individual data points are shown as grey spheres. **(D and E)** Representative ouabain-sensitive currents from two oocytes expressing WT (D) or Y780F (E). The currents were elicited by the pulse protocol illustrated in the box in two conditions: 125 mM Na^+ (top) and 62.5 mM Na^+ (bottom). The pulse protocol was repeated in the absence and then in the presence of ouabain, to obtain the subtracted ouabain-sensitive current displayed. **(F and G)** Q–V curves for the integral of the currents during the pulse (Q_{ON}), at 125 mM Na^+, and upon return to −50 mV (Q_{OFF}) at 125 mM Na^+ (solid) and 62.5 mM Na^+ (open) for WT (F) and Y780F (G) expressing oocytes displayed in D and E. Line plots are fits by Boltzmann distribution (Eq. 4) with parameters $V_{1/2}$ = −49.1 mV, kT/z_qe = 43.6 mV, Q_{tot} = 39.7 nC (Q_{ON} at 125 mM Na^+), $V_{1/2}$ = −38.2 mV, kT/z_qe = 39.1 mV, Q_{tot} = 35.7 nC (Q_{OFF} at 125 mM Na^+) and $V_{1/2}$ = −60.5 mV, kT/z_qe = 39.1 mV, Q_{tot} = 34 0.1 nC (Q_{OFF} at 62.5 mM Na^+) for WT, and $V_{1/2}$ = −119.6 mV, kT/z_qe = 56.8 mV, Q_{tot} = 16.8 nC (ON at 125 mM Na^+, fit to −160 mV only), $V_{1/2}$ = −121 mV kT/z_qe = 48 mV Q_{tot} = 16.3 nC (OFF at 125 mM Na^+) and $V_{1/2}$ = −131 mV kT/z_qe = 48 mV Q_{tot} = 14.5 nC (OFF at 62.5 mM Na^+), for Y780F. **(H)** Mean Q_{OFF}–V curves (normalized to Q_{tot} from Boltzmann equations) from oocytes expressing WT (black, n = 5) or Y780F (red, n = 8) where transient charge movement was evaluated in both 125 and 62.5 mM Na^+. Line plots are Boltzmann curves with parameters: $V_{1/2}$ = −42.0 mV, kT/z_qe = 35 mV at 125 mM Na^+ and $V_{1/2}$ = −67.6 mV, kT/z_qe = 35 mV for WT and $V_{1/2}$ = −113.5 mV, kT/z_qe = 51.8 mV at 125 mM Na^+ and $V_{1/2}$ = −144.8 mV, kT/z_qe = 51.8 mV at 62.5 mM Na^+, for Y780F. A shared slope factor (kT/z_qe) was used for the two concentrations in each mutant.

Q_{OFF}. The normalized Q_{OFF}–V curve (Fig. 3 H), fitted with a Boltzmann distribution, illustrates that halving the concentration of Na^+ shifts the center of the Q–V curve, $V_{1/2}$, toward more negative voltages in both WT (−24 ± 5 mV, SD, n = 5) and Y780F mutant (−33 ± 12 mV, SD, n = 8), consistent with similar experiments previously reported in *Xenopus* oocytes (Vedovato and Gadsby, 2010). Considering the linear dependence between the shift in $V_{1/2}$ and the fold change in Na^+ concentration (Holmgren and Rakowski, 2006), $V_{1/2}$ relates to the overall apparent affinity for external Na^+. Each ∼25 mV leftward shift in $V_{1/2}$ indicates an approximately twofold reduction in apparent affinity for external Na^+ (Meyer et al., 2020; Nielsen et al., 2019). Thus, Y780F

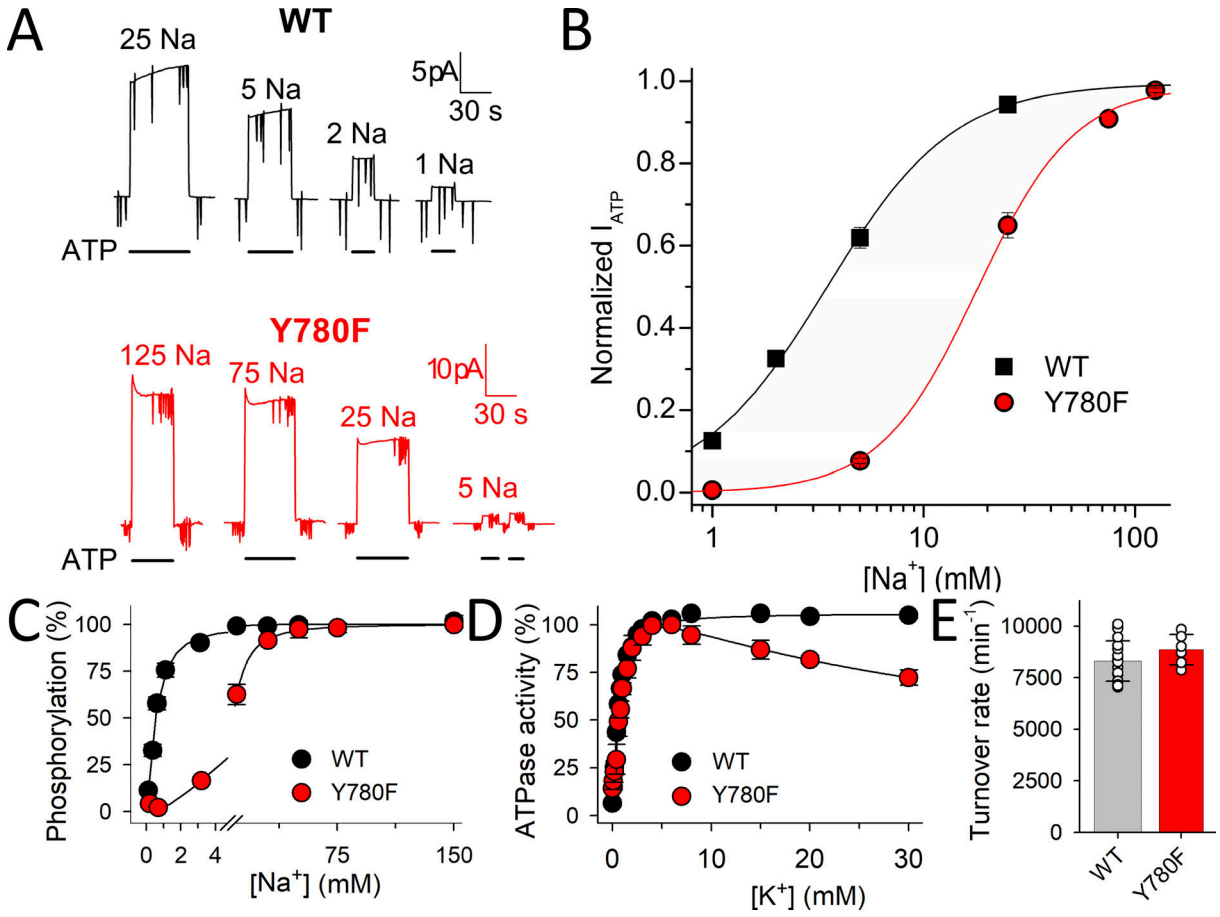

Figure 4. **Interaction with intracellular Na^+ and ATPase activity of WT and Y780F. (A)** ATP induced currents at 0 mV from two patches excised from two oocytes: one expressing WT pumps (top, black traces) and another expressing Y780F pumps (bottom, red traces). The patch pipettes contained extracellular $NMDG^+$ solution with 5 mM K^+ and the bath intracellular solution ($NMDG^+$ + Na^+ = 125 mM) with the indicated Na^+ concentration. **(B)** Mean normalized ATP-activated Na^+/K^+ pump currents from three patches as a function of the intracellular Na^+ concentration. Lines are fits of a Hill equation, with best fit parameters $K_{0.5}$ = 3.47 ± 0.25 mM, n_H = 1.4 ± 0.1 for WT and $K_{0.5}$ = 17.9 ± 0.96 mM, n_H = 1.9 ± 0.2 for Y780F. **(C)** Na^+ dependence of phosphorylation. Phosphorylation was carried out for 10 s at 0°C with 2 µM [γ-^{32}P]ATP in 20 mM Tris (pH 7.5), 3 mM $MgCl_2$, 1 mM EGTA, 10 µM ouabain, 20 µg oligomycin/ml, and the indicated concentration of Na^+ added as NaCl with various concentration of $NMDG^+$ to maintain constant ionic strength. Line plots represent the best fit of a Hill function (Eq. 1 in Materials and methods) with $K_{0.5}$ ± SD and the number of independent experiments reported in Table 1. **(D)** K^+ dependence of Na^+,K^+-ATPase activity determined at 37°C in 40 mM NaCl, 3 mM ATP, 3 mM $MgCl_2$, 30 mM histidine (pH 7.4), 1 mM EGTA, 10 µM ouabain, and the indicated concentration of K^+ added as KCl. Line plots represent the best fit of a double Hill function to the data (see Materials and methods), with $K_{0.5}$ ± SD and the number of independent experiments corresponding to the rising part reported in Table 1. For C and D, error bars (seen only when larger than the size of the symbols) represent SEM. **(E)** Turnover rate of WT and Y780F (mean ± SD) calculated as the ratio between the maximum ATPase activity (determined at 130 mM Na^+ and 20 mM K^+ under conditions otherwise similar to those for D) and the active site concentration (phosphorylation level obtained under stoichiometric conditions, i.e., as for C at 150 mM NaCl; Nielsen et al., 2019).

reduces extracellular Na^+ affinity by 11–20-fold (~86 mV shift). Y780F also increases the slope factor (shallower voltage dependence), an effect more difficult to interpret due to the complex relationship of the slope factor to sequential voltage-dependent reactions (Bezanilla and Villalba-Galea, 2013) similar to those reported for extracellular Na^+ binding to the pump (Hilgemann, 1994; Holmgren et al., 2000).

Interaction with intracellular ions was evaluated in giant patches excised from *Xenopus* oocytes and in membrane preparations from COS-1 cells (Fig. 4). Fig. 4 A shows currents from two patches excised from an oocyte expressing WT (top, black) and another expressing Y780F (bottom, red). With near-saturating 5 mM K^+ in the extracellular (intrapipette) $NMDG^+$ solution, activation of Na^+/K^+ pump current requires the presence of both Na^+ and ATP, allowing to obtain the Na^+-concentration dependence of ATP-activated current (Fig. 4 B). Y780F causes a sixfold reduction in apparent affinity for activation by intracellular Na^+. Since this apparent affinity for Na^+ is influenced by the distribution of the major conformational states, E1 forms (which bind Na^+ from the intracellular side to activate phosphorylation of the pump) and E2 forms (which bind K^+ from the extracellular side to activate dephosphorylation, cf. Fig. 1 A), we also measured the apparent affinity for Na^+ under conditions that favor the accumulation of E1 forms in the absence of K^+ to more closely reflect the intrinsic affinity of E1 for Na^+. This was accomplished by determining the Na^+ dependence of the phosphorylation reaction in plasma membrane preparations from COS-1 cells expressing either WT rat α_1 or the Y780F

mutant (Fig. 4 C). The membrane vesicles were made leaky to allow ligand access to the Na^+/K^+ pump from both sides of the membrane (see Materials and methods). Oligomycin blocks the transition from E1P to E2P, locking the pump in E1 forms. Therefore, in the presence of 2 μM [γ-^{32}P]ATP with oligomycin, the phosphorylation assay exclusively reflects interaction with intracellular-facing sites, even though Na^+ was applied to both sides of the membrane. As seen in Fig. 4 C, Y780F causes a 16-fold reduction in affinity for intracellular Na^+, identical to its effect on extracellular Na^+ affinity described in Fig. 3.

The ATPase activity as a function of K^+ concentration was also evaluated (Fig. 4 D). In WT pumps, the K^+ dependence is monophasic, but there is a biphasic response in Y780F membranes: a rising phase, which corresponds to the activation of ATPase activity by interaction at extracellular-facing sites stimulating dephosphorylation, and an inhibitory phase, which represents stronger K^+ competition with Na^+ for intracellular-facing sites (inhibiting the phosphorylation reaction) due to a larger reduction in affinity for Na^+ than for K^+, just as observed for extracellular-facing sites. Furthermore, the $K_{0.5,K}$ for K^+ activation of ATPase activity extracted from the rising phase shows a 1.4-fold increase relative to WT, again, matching the 1.5-fold increase observed in electrophysiological experiments in the presence of Na^+ (Fig. 3 C). Finally, the turnover rate, calculated as the maximum ATPase activity divided by the number of sites in the membrane preparation (Fig 4 E), is not altered by the Y780F mutation. Overall, removal of the hydroxyl group reduces the affinity for Na^+ by 16-fold on both sides of the membrane in the absence of K^+ and the affinity for K^+ on the external side by 6.4-fold in the absence of Na^+ (only 1.5-fold in the presence of Na^+).

The effects of the non-conservative Y780L (hydrophobic side chain), Y780Q (hydrophilic side chain of similar length), and Y780A (minimal side chain) mutations were also evaluated using both electrophysiological assays (except for patch-clamp) and biochemical assays. Using TEVC, we evaluated the K^+-concentration dependence of pump current activation in the absence or presence of external Na^+ (Fig. 5, A and B) and the changes in apparent affinity for external Na^+ in the voltage dependence of transient charge movement without external K^+ (Fig. 5, C and D). Y780L shows large outward currents, while Y780A and Y780Q show reduced maximal pump current in $NMDG^+$ (Fig. 5 A). Their effects on the $K_{0.5,K}$ for activation of pump current both in the absence and presence of Na^+ are summarized in Fig. 5 B. All three mutations reduce the apparent affinity ($1/K_{0.5}$) for external K^+ in the absence of Na^+. Like WT, Y780Q shows an approximately fivefold larger $K_{0.5,K}$ in Na^+ due to competition between the transported ions, Na^+ and K^+. In contrast, the $K_{0.5,K}$ for Y780A is only slightly affected by Na^+, indicating that Y780A, like Y780F, has a larger reduction in apparent affinity for Na^+ than for K^+. The ouabain-sensitive transient currents induced by 50 ms-long voltage pulses in 125 mM Na^+, without K^+ (Fig. 5 C), were integrated to obtain the Q_{OFF}–V plots, which were fitted with a Boltzmann distribution (Fig. 5 D) with parameters given in the figure legend. Of note, the charge movement of the Y780L mutant is spread out across a wide voltage range making it impossible to fit this mutant's Q–V curve with a Boltzmann. The total charge moved is reduced for Y780A and Y780Q, indicating reduced expression of these mutants, which partially explains the reduced pump currents in Fig 5 A. The plot of the normalized Boltzmann functions fitted to the average data (Fig. 5 D, insert) illustrates the increased slope factor and altered $V_{1/2}$ caused by all mutations. Y780A shows a larger reduction in apparent affinity for Na^+ (approximately −129 mV shift, consistent with a 36–87-fold reduction, although a precise determination is impossible due to the reduced size of the transients and the strong leftward shift) than that already described for Y780F (−86 mV, 11–20-fold reduction). In contrast, Y780Q increases the apparent affinity for Na^+, shifting the curve to the right (approximately +20 mV, approximately twofold increase in apparent affinity for external Na^+). Table 1 summarizes the $V_{1/2}$ and $K_{0.5,K}$ for WT, Y780F, Y780L, Y780Q, and Y780A.

The effects of the substitutions Y780/L/Q/A on Na^+ interaction on the intracellular side, as well as other partial reactions, were further evaluated biochemically (Fig. 6 and Table 1) in plasma membrane preparations from COS-1 cells expressing the rat α1 mutants. As described above for Y780F, the Na^+ concentration dependence of phosphorylation in the presence of [γ-^{32}P]ATP and oligomycin and the absence of K^+ (Fig. 6 A) evaluates the affinity of the intracellular-facing sites of the E1 form for Na^+. Y780A and Y780L, like Y780F, reduce the apparent affinity (increase $K_{0.5}$) for Na^+ by 48- and 12-fold, respectively, whereas Y780Q increases the apparent affinity by twofold, thus quantitatively matching the effects on extracellular Na^+ affinity determined in the electrophysiological measurements for Y780A and Y780Q. The fact that Y780L reduces Na^+ affinity less than Y780F provides a clear demonstration that Na^+–π interaction with the phenol ring at position 780 contributes minimally, if at all, to the binding of Na^+. The K^+ dependence of ATPase activity in the presence of Na^+ (Fig. 6 B), reflecting the activation of dephosphorylation by K^+ binding to extracellular-facing sites, is WT-like for Y780L, whereas Y780Q and Y780A show approximately four- and approximately threefold reduced apparent K^+ affinities, respectively, relative to WT. It was further observed that high concentrations of K^+ exert an inhibitory effect on the ATPase activity of mutants Y780A and Y780L, as described above for Y780F. By contrast, such inhibition was not observed for Y780Q, which behaves like WT in this respect. The larger reduction in Na^+ affinity than in K^+ affinity seen for Y780F/A/L explains the inhibitory phase observed at high K^+ concentrations in these mutants by a reduced ability of Na^+ to compete with K^+ at the intracellular-facing sites. The effects on K^+ interaction were further analyzed by studying the K^+ concentration dependence of the phosphorylation level (Fig. 6 C). K^+ reduces the phosphorylation level both by competing with Na^+ for binding to intracellular-facing sites of the E1 form, driving the enzyme backward into the K^+-occluded E2($2K^+$) form by what has been termed the "direct route" (Glynn, 1993), and by binding to the extracellular-facing sites, activating dephosphorylation of E2P. Both routes lead to the K^+-occluded E2($2K^+$) form. The apparent affinity for K^+ in this assay is higher than the apparent affinity for K^+ in the Na^+,K^+-ATPase assay (Fig. 6 A and Table 1) because the high ATP concentration in the ATPase assay (3 mM ATP

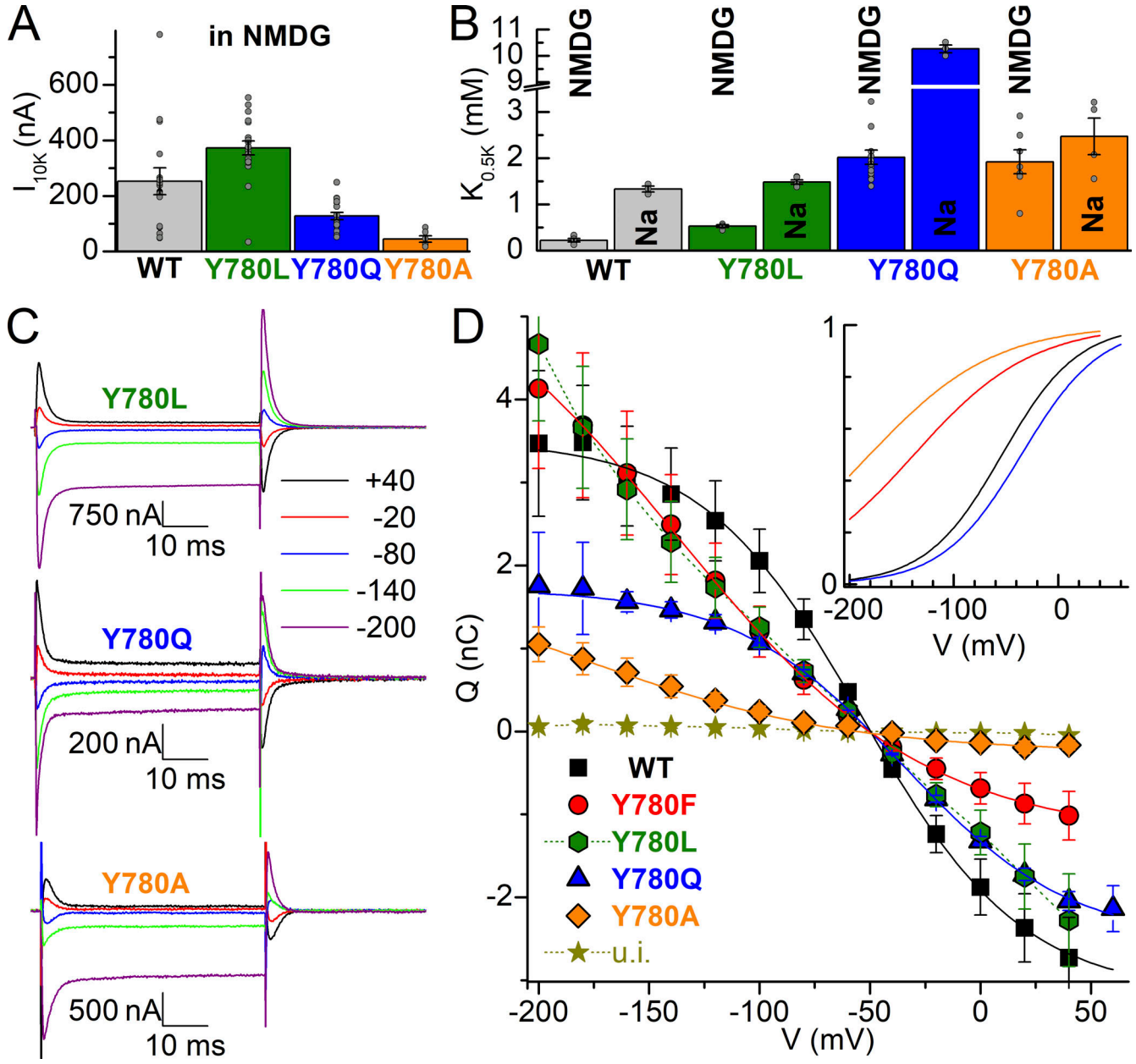

Figure 5. **Interaction of Y780L/Q/A with extracellular ions. (A)** Na^+/K^+ pump current induced by 10 mM K^+ in $NMDG^+$. **(B)** $K_{0.5,K}$ obtained from Hill fits (Eq. 2) to the K^+-induced current at −50 mV in $NMDG^+$ or with 125 mM Na^+. Grey circles show each independent measurement in individual oocytes. **(C)** Representative ouabain-sensitive currents elicited by 50-ms-long pulses from −50 mV to the indicated voltages, in oocytes bathed by 125 mM Na^+ solution, expressing Y780L, Y780Q, or Y780A. **(D)** Mean Q_{OFF}–V curve from 6 to 12 experiments. Continuous lines are Boltzmann distribution fits to the average data, with kT/z_qe = 36 mV and Q_{tot} = 6.65 nC for WT and kT/z_qe = 50 mV; Q_{tot} = 7.32 nC for Y780F, kT/z_qe = 45 mV, Q_{tot} = 4.24 nC for Y780Q and kT/z_qe = 60 mV, Q_{tot} = 2.24 nC (Y780A). The mean $V_{1/2}$ from individual experiments is listed in Table 1. The inset shows normalized Boltzmann equations to illustrate shifts in Q–V, except for Y780L which could not be fit, see Results.

versus 2 µM in the phosphorylation assay) destabilizes E2($2K^+$) (see below in relation to the ATP concentration dependence of ATPase activity). Thus, the phosphorylation inhibition assay reflects the affinity of the sites for K^+ in combination with the stability of the occluded E2($2K^+$) form. As was the case with the results from the other assays for K^+ affinity, the fold-change in apparent affinity for K^+ inhibition of phosphorylation is largest for Y780A and Y780Q (Fig. 6 C and Table 1), indicating that the interaction with K^+ is particularly weakened in these two mutants. The turnover rate for ATP hydrolysis, determined as the maximal ATP hydrolysis rate relative to the site concentration (phosphorylation level under stoichiometric conditions), is decreased for Y780Q and Y780A (Table 1), which may reflect a defective activation by K^+ of the E2P dephosphorylation. Thus, the lower maximal pump current observed with these mutants (Fig. 5 A) probably reflects both their reduced expression (estimated from total charge moved in the Q–V curves) and reduced maximal turnover rate.

Table 1. **Functional parameters of Y780 mutants**

	Turnover rate	$K_{0.5,\ Na+}$ phosphorylation	$K_{0.5,\ K+}$ ATPase activity	$K_{0.5,K+}$ inhibition of phosphorylation	E_2P fraction/ dephosphorylation rate in Na^+	$K_{0.5,K+}$ I_P in $NMDG^+$	$K_{0.5,K+}$ I_P in Na^+	$V_{1/2}$
	s^{-1}	mM	mM	μM	$\%/s^{-1}$	mM	mM	mV
WT	138 ± 16 (16)	0.50 ± 0.08 (17)	0.57 ± 0.09 (14)	96 ± 12 (3)	41 ± 8 (8) 0.14 ± 0.02	0.22 ± 0.09 (6)	1.3 ± 0.1 (3)	−51 ± 8 (8)
Y780A	61 ± 9 (12)	24.0 ± 3.3 (6) 48-fold ↑	1.8 ± 0.6 (8) 3.2-fold ↑	376 ± 118 (3) 3.9-fold ↑	37 ± 9 (3) 0.07 ± 0.03	1.9 ± 0.7 (4) 8.6-fold ↑	2.5 ± 0.8 (4) 1.9-fold ↑	−180* (6) 36–87-fold↑
Y780L	137 ± 43 (16)	6.0 ± 0.6 (2) 12-fold ↑	0.63 ± 0.11 (6) 1.1-fold ↑	126 ± 37 (4) 1.3-fold ↑	48 ± 5 (2) 0.11 ± 0.002	0.53 ± 0.06 (4) 2.4-fold ↑	1.5 ± 0.1 (5) 1.2-fold ↑	ND
Y780F	148 ± 12 (6)	8.1 ± 2.0 (6) 16-fold ↑	0.78 ± 0.13 (3) 1.4-fold ↑	159 ± 56 (3) 1.7-fold ↑	42 ± 20 (4) 0.22 ± 0.01	1.4 ± 0.5 (8) 6.4-fold ↑	2.0 ± 0.7 (4) 1.5-fold ↑	−137 ± 13 (12) 11–20 fold↑
Y780Q	81 ± 8 (6)	0.25 ± 0.05 (9) 2-fold ↓	2.5 ± 0.3 (5) 4.4-fold ↑	422 ± 41 (3) 4.4-fold ↑	45 ± 10 (3) 0.04 ± 0.02	2.0 ± 0.7 (18) 9.1-fold ↑	10.3 ± 0.3 (3) 7.7-fold ↑	−33 ± 13 (6) 1.7–1.9-fold ↓

The data were extracted from results in Figs. 3, 4, 5, 6, and 7, except the turnover rates of Y780A/L/Q, which were obtained as described in Fig. 4 E. The K^+-inhibition of phosphorylation of Y780F was carried out as described for WT and the other mutants in the legend to Fig. 6 C. Average values are indicated with SD and number of determinations in parentheses, except in the case marked by *, where fit to average data was applied. Range of fold changes in $K_{0.5}$ for external Na^+ given a shift in $V_{1/2}$ was obtained, based on 25 mV/twofold change and ∼20 mV/twofold change (based on results from Holmgren and Rakowski, 1994; Holmgren and Rakowski, 2006; Vedovato and Gadsby, 2010, and consistent with our data in Fig. 3 F).

Changes in apparent affinities for transported ions may reflect that a mutation alters the distribution between the phosphoenzyme intermediates E1P(3Na^+) and E2P instead of direct effects on ion binding. We analyzed the distribution of phosphoenzyme intermediates by taking advantage of the ADP-sensitivity of the E1P(3Na^+) conformation (Fig. 7 A and Table 1). When ADP is added to the phosphoenzyme (previously formed in the presence of [γ-^{32}P]ATP and Na^+, but the absence of K^+), two clearly distinguishable phases of the dephosphorylation reaction are observed. The rapid phase reflects E1P(3Na^+), donating the phosphoryl group back to ADP, forming ATP, whereas the slow phase reflects the dephosphorylation of E2P in the absence of K^+ (Fig. 1 A). The E2P dephosphorylation occurs at much slower rates when Na^+ interacts than when K^+ interacts with sites I and II. The relative amplitude of the slow phase reflects the E2P level and was almost unaffected by all four mutations (Fig. 7 A and Table 1), indicating negligible effects on the E1P(3Na^+)–E2P distribution.

Finally, we evaluated the E2(2K^+) → E1 transition of the dephosphoenzyme by studying the ATP concentration dependence of ATPase activity in the presence of both Na^+ and K^+ (Fig. 7 B). ATP acts at two steps in the pump cycle—binding with high affinity (<1 μM) to the E1 conformation, phosphorylating the enzyme in the presence of Na^+, and binding with low affinity (>50 μM) to the K^+-occluded E2(2K^+) form, accelerating the E2(2K^+) → E1 transition that deoccludes and releases K^+ to the intracellular side (Post et al., 1972; Stanley et al., 2016). Because of the latter effect, the apparent affinity for ATP in the activation of Na^+,K^+-ATPase activity increases if the E2(2K^+) → E1 step is accelerated by a mutation (Holm et al., 2015). Compared with the WT, Y780A and Y780Q, the two mutations with a strong effect on affinity for external K^+ in the absence of Na^+ interference (a ninefold reduction, Fig. 5 B), show a marked increase (six- and threefold, respectively) in the apparent affinity for ATP, whereas mutants Y780L and Y780F (with a two- and a sixfold reduction of affinity for external K^+, respectively), behave closer to WT. The enhanced apparent affinity for the ATP of Y780A and Y780Q can be explained by their weakened interaction with K^+ in the occluded E2(2K^+) state, thus accelerating K^+ deocclusion.

We also used TEVC to test the effect of six other side chains capable of hydrogen bonding: Y780C/S/T/H/D/E. The two mutants with carboxylic acid substituents, Y780D (n = 14, three batches of oocytes) and Y780E (n = 10, two batches of oocytes), lacked K^+-induced outward currents, ouabain-sensitive transient currents, or leak currents in the absence of K^+, indicating a lack of expression. Fig. 8 shows that the center of the Q–V curves of Y780C/S/T/H is positioned between Y780F and WT, indicating reduced Na^+ affinity (Fig. 8, A–C), and that the apparent affinity for K^+ is reduced, as well, compared with WT, both in the absence (Fig. 8 D) and in the presence (Fig. 8 E) of external Na^+. The equivalent histidine (Y768H) and cysteine (Y768C) substitutions in the α3 subunit are associated with AHC (Panagiotakaki et al., 2015). Since a depolarizing inward current through the mutant pumps has been implicated in the pathogenesis of some neurological disease-causing Na^+/K^+ pump mutations (see Discussion), we measured the steady-state ouabain-sensitive current in the presence of Na^+ at different K^+ concentrations and voltages (Fig. 8 F). In contrast to WT (left panel), the two α3-disease-equivalent mutants (center and right panels) display inward currents at negative voltages in the absence of K^+ (also seen in Fig. 8 A). However, the current of the mutants is outward, albeit of much smaller amplitude, at K^+ concentrations above 3 mM (the lowest normal

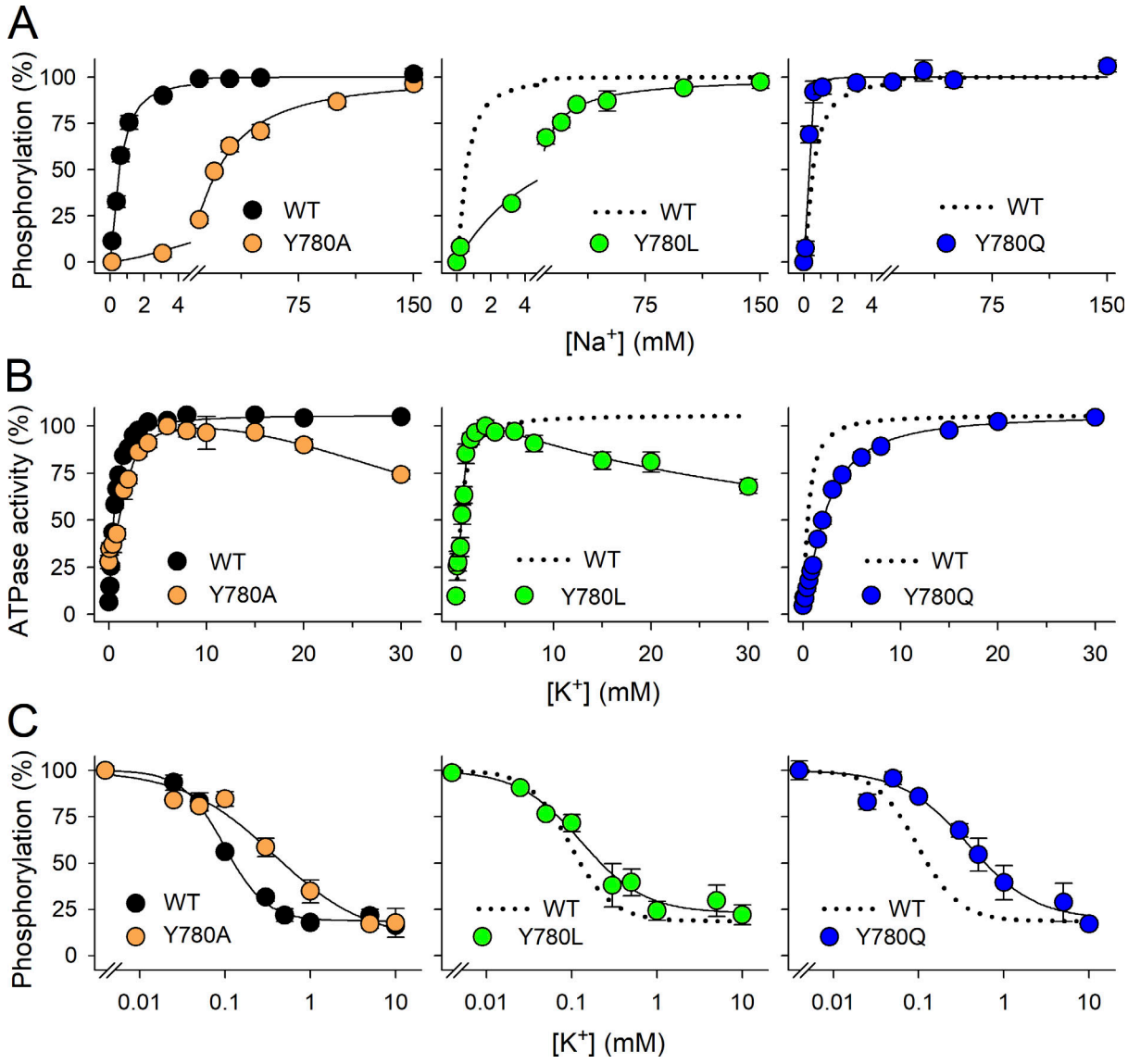

Figure 6. **Ion concentration dependence of phosphorylation and ATPase activity. (A)** Na^+ dependence of phosphorylation determined as described in Fig. 4 C. Line plots represent the best fit of a Hill function (Eq. 1) with $K_{0.5}$ ± SD and number of independent experiments reported in Table 1. **(B)** K^+ dependence of Na^+,K^+-ATPase activity determined as in Fig. 4 D. Line plots represent the best fit of a double Hill function to the data (see Materials and methods), with $K_{0.5}$ ± SD and number of independent experiments corresponding to the rising part reported in Table 1. **(C)** K^+ affinity determined by K^+ inhibition of phosphorylation. Phosphorylation was carried out as in A, with 100 mM NaCl and the indicated concentration of K^+ added as KCl (with various concentrations of choline chloride to maintain a constant ionic strength), but without oligomycin. Line plots represent the best fit of a negative Hill function (Eq. 2). The extracted $K_{0.5}$ values ± SD and the number of independent experiments are reported in Table 1. For all panels, error bars (seen only when larger than the size of the symbols) represent SEM.

physiological K^+ concentration). Therefore, it seems unlikely that a gain-of-function passive inward current is the mechanism by which these two mutations cause disease, although this could be different in α3 pumps.

All experiments so far suggest that the hydrogen-bond interactions at position 780 are critically important to determine the apparent affinity for Na^+ on both sides of the membrane. A weakness of conventional mutation is its general inability to alter specific chemical interactions without concomitant, substantial changes in amino acid shape. To specifically evaluate the importance of the aromaticity of tyrosine, we used non-sense suppression to incorporate subtle modifications of the aromatic sidechain (Infield et al., 2018; Leisle et al., 2015; see Materials and methods). First, we tested the feasibility of this approach to express functional Na^+/K^+ pumps (Fig. 9). We co-injected the cRNA with the tag stop codon at position 780, together with the *Pyl*-tRNA loaded with tyrosine or phenylalanine, and this was followed by a boost injection of tRNA each day until recording. We measured the current activated by the addition of 10 mM K^+ and the transient charge moved in presence of Na^+ without K^+, 3 and 4 d after injection. The K^+-induced current (Fig. 9, A and B) and the total charge (Fig. 9 C) were approximately fivefold reduced in oocytes expressing the non-sense–suppressed tyrosine (NSS-Tyr) or phenylalanine (NSS-Phe), relative to oocytes

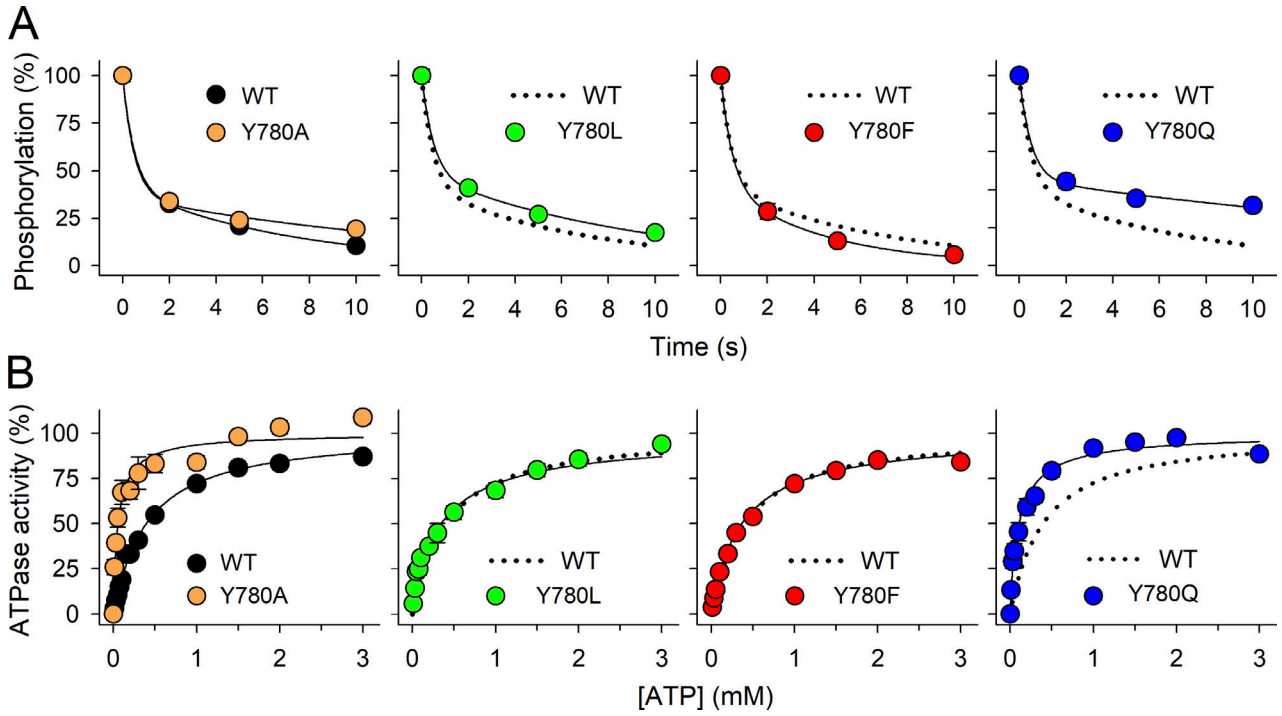

Figure 7. **E1P(3Na⁺)–E2P distribution evaluated by ADP sensitivity and E2(2K⁺) → E1 conformational transition evaluated by ATP dependence of Na⁺,K⁺-ATPase activity. (A)** ADP-dependent dephosphorylation. Phosphorylation was carried out for 5 s at 0°C with 2 µM [γ-^{32}P]ATP in 20 mM Tris (pH 7.5), 100 mM NaCl, 50 mM choline chloride, 3 mM $MgCl_2$, 1 mM EGTA, and 10 µM ouabain. Dephosphorylation was initiated by the addition of 2.5 mM ADP and 1 mM unlabeled ATP. The dephosphorylation reaction was terminated by acid quenching after the indicated time intervals. Line plots represent the best fit of a bi-exponential decay function (Eq. 3 in Materials and methods) with the rate constant corresponding to the rapid phase, reflecting the ADP reaction with E1P, set to 2 s^{-1}. The relative fraction of E2P together with the rate constant corresponding to the slow phase, reflecting E2P dephosphorylation, are indicated in Table 1 as mean ± SD and number of independent experiments. **(B)** ATP dependence of Na⁺,K⁺-ATPase activity. ATPase activity was determined at 37°C in 130 mM NaCl, 20 mM KCl, 3 mM $MgCl_2$, 30 mM histidine (pH 7.4), 1 mM EGTA, 10 µM ouabain, and the indicated ATP concentrations. Line plots represent the best fit of a Hill function (Eq. 1 in Materials and methods). $K_{0.5}$ values (in µM ± SD) and number of experiments (*n*) in parentheses are: WT, 402 ± 74 (12); Y780A, 63 ± 20 (6); Y780L, 362 ± 122 (4); Y780F, 368 ± 19 (4); Y780Q, 121 ± 61 (7). In all panels, symbols are mean ± SEM (seen only when larger than the symbols). For each assay, the WT data from the left panel is reproduced as broken lines in the other panels.

injected with WT or Y780F cRNA, but the kinetic parameters ($K_{0.5,K}$ and voltage dependence) of both non-sense–suppressed natural amino acids were identical to WT or Y780F pumps (Fig. 9, B and C), thus validating the approach. 22 out of 27 NSS-Tyr-injected oocytes tested showed pump currents (11 batches). Similarly, 32 out of 38 NSS-Phe-injected oocytes showed pump currents (11 batches).

We injected several phenylalanine analogs (recall tyrosine is 4-hydroxyphenylalanine or *p*-OH-Phe with the hydroxyl group at the *para* position) previously used with ion channels (Ahern et al., 2008; Pless et al., 2011a; Santarelli et al., 2007; Tian et al., 2016), 3-fluorotyrosine (*m-F*-Tyr; with fluorine at the *meta* position), 4-fluorophenylalanine (*p-F*-Phe), 3,5-difluorphenyla lanine (di-*m-F*-Phe, with fluorine groups at both *meta* positions), 4-bromophenylalanine (*p*-Br-Phe), 4-hydroxycyclohexylalanine (CHO), and cyclohexylalanine (CHA) and measured K⁺-induced currents in oocytes held at −50 mV, 4 d after injection (Fig. 10). The quality of the cRNA Y780*tag*–α1β3 mixtures used for these studies was always tested prior to the experiment utilizing tRNAs that incorporate into clearly functional pumps (NSS-Tyr, NSS Phe, *m-F*-Tyr or *p-F*-Phe). Uninjected oocytes and oocytes injected with CHA or with the unloaded tRNA (pdCpA) show very small inward currents (<10 nA amplitude) due to non-Na⁺/K⁺ pump currents (Fig. 10 A); oocytes injected with *p*-Br-Phe and CHO show currents not significantly different from zero (P = 0.33 and P = 0.35, respectively), probably reflecting minimal expression. Small outward currents were observed in di-*m-F*-Phe injected oocytes and robust outward currents were observed in oocytes injected with *m-F*-Tyr, *p-F*-Phe. The apparent affinity for K⁺ in the absence of Na⁺ (Fig. 10 B) is fivefold reduced in *p-F*-Phe compared with phenylalanine, while *m-F*-Tyr shows only a minor (twofold) reduction of apparent affinity for K⁺ compared with tyrosine (dose responses could not be analyzed in di-*m-F*-Phe–injected oocytes due to tiny outward currents). We could not determine if the lack of outward current in di-*m-F*-Phe is due to reduced K⁺ interaction or simply due to the apparent reduction in expression levels. (As the 10 mM K⁺-induced currents in this mutant were frequently <10 nA currents, we chose to determine the pump-specific ouabain-sensitive transient charge movement which was also tiny, but less prone to errors due to small changes in leak and/or K⁺ conductance.)

To determine Na⁺ interaction as previously described for the natural mutants, we measured Na⁺/K⁺ pump-specific ouabain-sensitive transient currents in oocytes that showed outward K⁺-induced currents larger than 7 nA, including di-*m-F*-Phe (Fig. 11). The analysis from independent experiments (with slightly

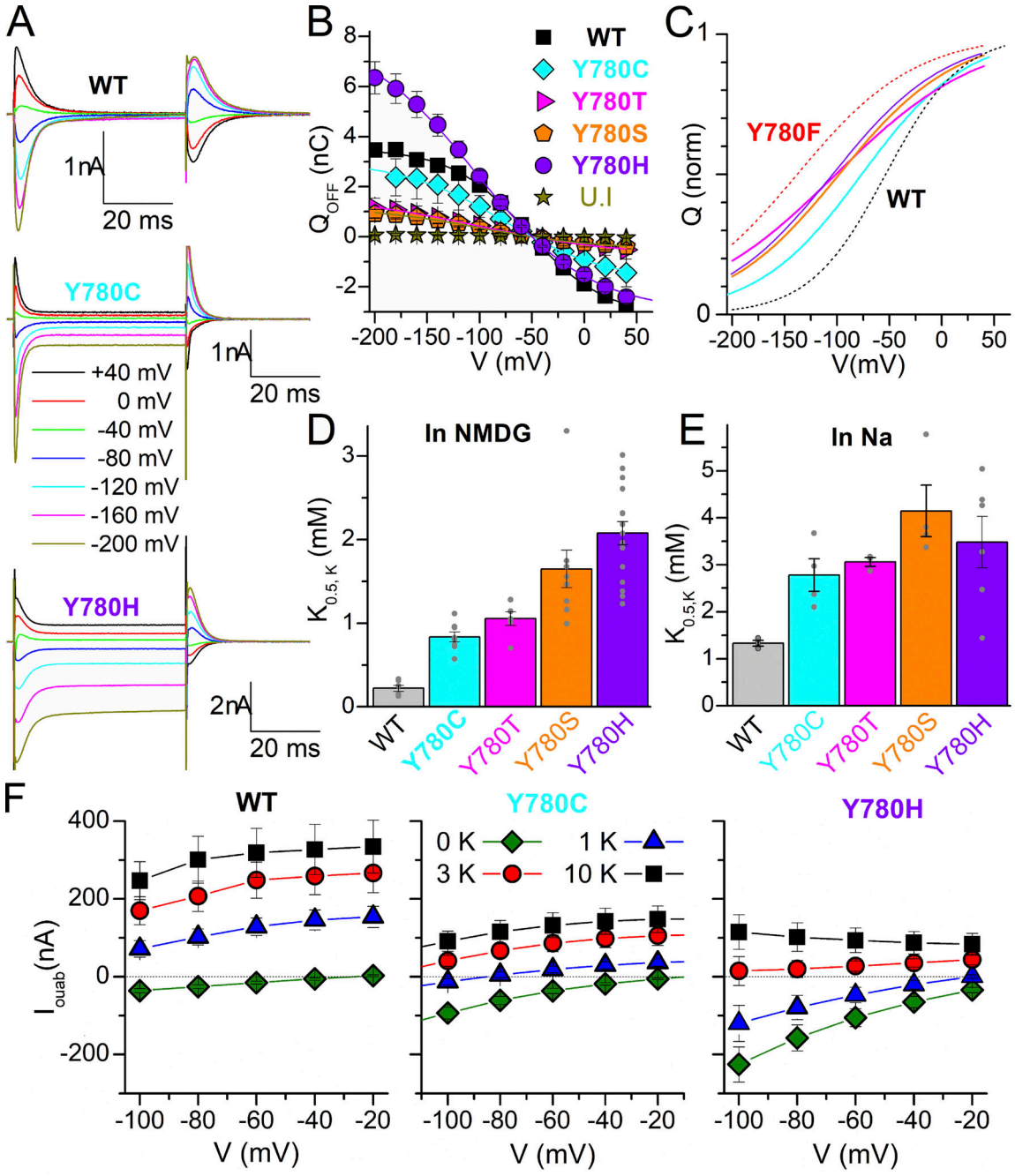

Figure 8. **Electrophysiological characteristics of Y780C, Y780T, Y780S, and Y780H. (A)** Ouabain-sensitive currents in 125 mM Na^+, elicited by 50 ms pulses to the indicated voltages. **(B)** Mean Q–V curve, obtained from the integral of the transient currents when the voltage returns to −50 mV, for WT, Y780C, Y780T, Y780S, and Y780H. **(C)** Normalized fitted curves from B, to illustrate changes in the Boltzmann distributions fitted to the mean data, with centers $V_{1/2}$ = −54 mV for WT, $V_{1/2}$ = −75 mV for Y780C, $V_{1/2}$ = −98 mV for Y780S, $V_{1/2}$ = −101 mV for Y780T, and $V_{1/2}$ = −104 mV for Y780H. WT and Y780F are shown as black and red dotted lines, respectively. **(D and E)** $K_{0.5}$ for K^+ activation of pump current when applied in $NMDG^+$ external solution (D) or Na^+ solution (E). Grey circles show individual data points from each oocyte. **(F)** Current–voltage relationship for the ouabain-sensitive currents in 125 mM Na^+ at four K^+ concentrations, for WT (left, *n* = 12) and the disease-causing Y780C (center, *n* = 2) and Y780H (right, *n* = 7). The dotted line marks the 0-current level.

different values than the fits to the average data) also shows that the charge for *m-F*-Tyr has a nearly identical center, $V_{1/2}$ = −55 ± 14 mV (*n* = 8, SD), to tyrosine (see Table 1), while *p-F*-Phe and di-*m-F*-Phe are centered respectively at $V_{1/2}$ = −166 ± 20 mV (*n* = 7, SD) and $V_{1/2}$ −141 ± 29 (*n* = 4, SD), the latter being very similar to Phe (see Table 1 and Fig. 11 C). Therefore, Na^+ interaction is unaltered by the reduction of the putative cation–π interaction strength through mono- and difluorination. The mild effects of fluorination of phenylalanine at position 780 contrasts with strong effects previously described in ion channels, where each fluorination event induces additive effects on the energetics of either gating (Pless et al., 2011b) or ligand binding (Ahern et al., 2008; Ahern et al., 2006; Pless et al., 2011a; Santarelli et al., 2007; Zhong et al., 1998).

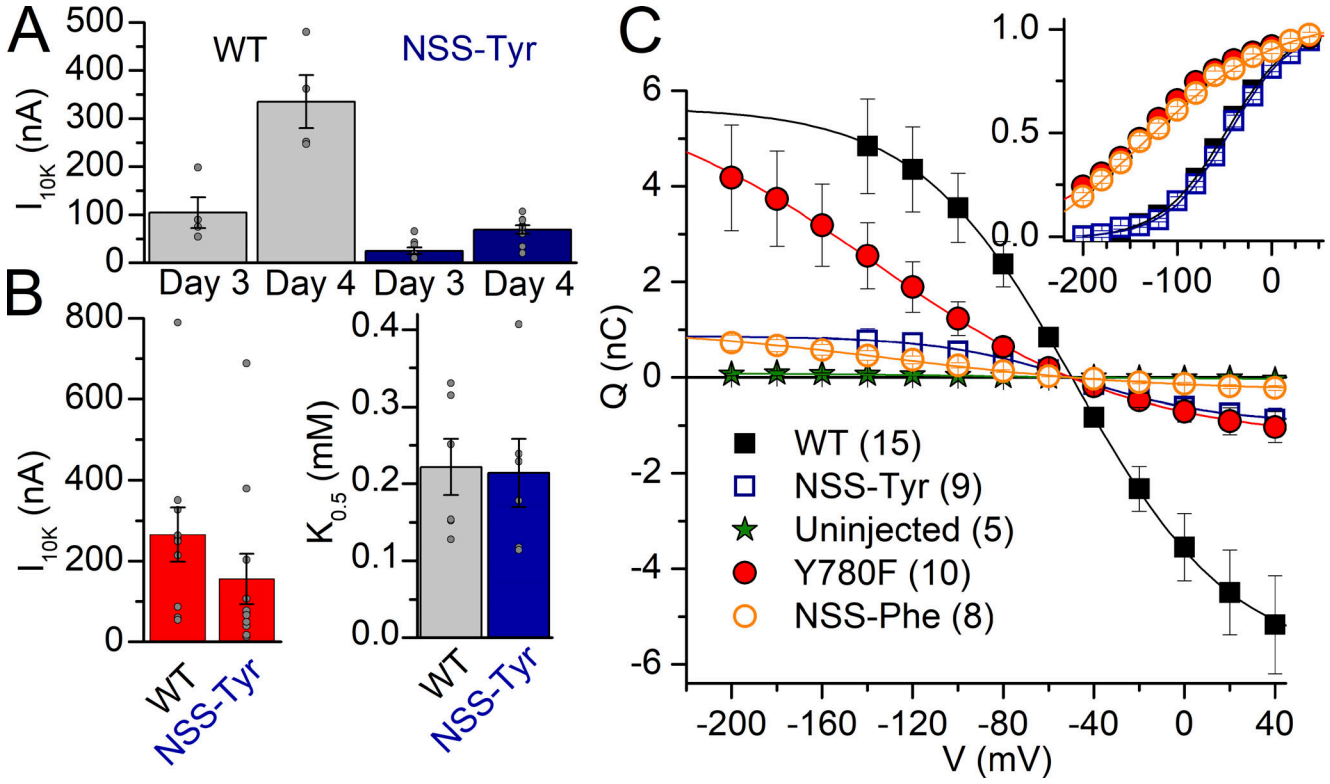

Figure 9. **Feasibility of non-sense suppression to express Na^+/K^+ pumps. (A)** Mean current induced by 10 mM K^+ 3 or 4 d after injection with either WT cRNA or Y780*tag* mutant cRNA + Tyr-tRNA (NSS-Tyr). The same batches of oocytes were tested on days 3 and 4 after injection. The pump current in oocytes expressing NSS-Tyr was smaller than WT, whether 3 or 4 d after injection. **(B)** Mean current induced by 10 mM K^+ in the absence of Na^+ (left) and apparent dissociation constant $K_{0.5,K}$ (right) from Hill fits in dose–response curves for K^+ activation at −50 mV in $NMDG^+$ 4 d after injection. Grey circles show individual data points in different oocytes. **(C)** Mean Q_{OFF}–V curves measured (125 mM Na^+, 0 K^+) for uninjected oocytes and for oocytes injected with WT cRNA, Y780F cRNA, Y780*tag* cRNA + Tyr-tRNA (NSS-Tyr), or Y780*tag* cRNA + Phe-tRNA (NSS-Phe). The line plots are the fits to Boltzmann distributions. The inset shows the mean normalized curves illustrating identical voltage dependencies for both pairs: WT NSS-Tyr and Y780F NSS-Phe.

Discussion

Central aspects of Na^+ and K^+ binding to the Na^+/K^+ pump have remained unclear, even after the enlightenment brought by the Na^+/K^+ pump crystal structures. Inspired by the important roles of aromatic residues in ion channels, in the present study, we have investigated the function of the highly conserved tyrosine residue of the fifth transmembrane segment (Y780 in *Xenopus* α1 and so numbered in this article) as a determinant of ion binding to the Na^+/K^+ pump and dissected the roles of Y780's distinct chemical components. First of all, the combination of electrophysiology and biochemistry allowed us to demonstrate that the effects of Y780 mutations on the apparent Na^+ affinity are independent of whether Na^+ reaches its transport sites from the intracellular side or the extracellular side. In both cases, the bound Na^+ ions become occluded upon binding. Therefore, we conclude that Y780 is a crucial residue for Na^+ interaction in the occlusion cavity.

The crystal structure of the Na^+/K^+ pump in the Na^+-bound E1 conformation (Kanai et al., 2013; Fig. 1 C) suggests that Y780 contributes both directly and indirectly to Na^+ interaction at the Na^+-specific site III. The bound Na^+ appears to interact directly with the backbone carbonyl of Y780, as well as through a putative cation–π interaction with the phenol ring, which forms a lid-like structure above the Na^+ ion at site III, giving the impression of acting as the ceiling of the binding/occlusion cavity (Kanai et al., 2013). Importantly, the crystal structure also shows that Y780 participates in a hydrogen-bonding network with several residues that directly coordinate Na^+ at site III. The side-chain hydroxyl group of Y780 hydrogen bonds with the backbone carbonyl of T816, thereby fixing the unwound part of M6, which in turn constrains the juxtaposed D817 that provides crucial side-chain oxygen ligands for the Na^+ ions at both site I and site III (Kanai et al., 2013), and with the side chain of Q932, which likewise is crucial to Na^+ interaction at site III (Kanai et al., 2013; Nielsen et al., 2019). The hydrogen bond network surrounding Na^+ site III further includes a bond between Q932 and the side chain of T816, whose indirect importance for Na^+ binding was previously demonstrated by mutagenesis (Vilsen, 1995). Consequently, Y780 appears to stabilize Q932, and thus the Na^+ at site III, in more than one way. By examining a series of mutants with natural and unnatural amino acids, we were able to distinguish the separate impacts of the chemical groups of Y780's side chain.

The marked 12-fold reduction in apparent affinity for Na^+ for Y780L (without the aromatic ring in the side chain) and 16-fold reduction for Y780F (with a phenol ring), corresponding to a change in Na^+ binding energy of $\Delta\Delta G \sim +6$ kJ/mol and $\sim +7$ kJ/mol, respectively ($\Delta\Delta G = RT\ln[K_{0.5}\text{mutant}/K_{0.5}\text{WT}]$), suggest

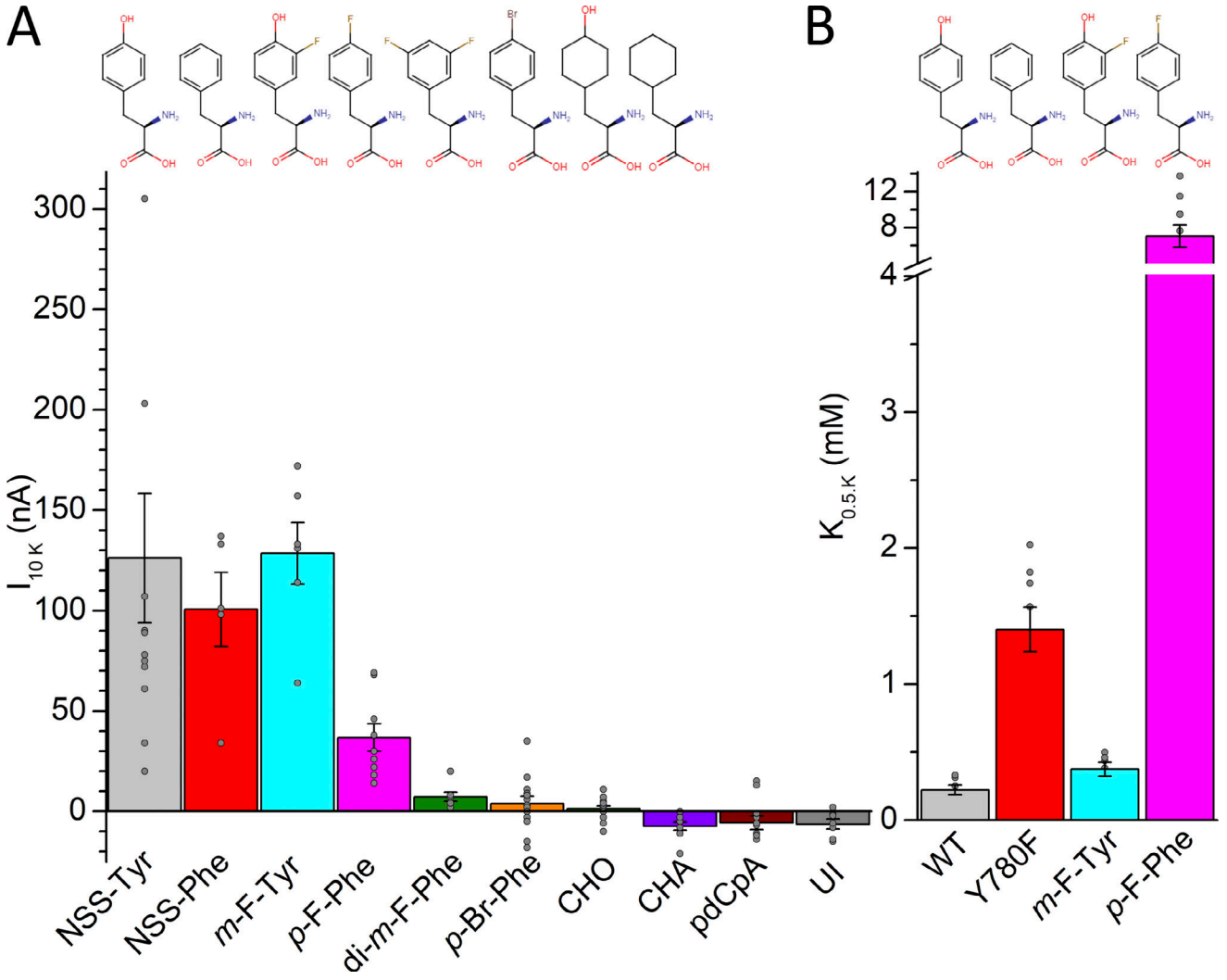

Figure 10. **K⁺-activated pump current with unnatural amino acids at position 780. (A)** Mean 10 mM K⁺-induced current in oocytes injected with Y780*tag* cRNA and tRNAs for tyrosine (NSS-Tyr), phenylalanine (NSS-Phe), and other phenylalanine derivatives. The label pdCpA designates the full-length ligated (but unacylated) tRNA control (see Materials and methods). **(B)** Mean $K_{0.5,K}$ for substitutions with large enough pump currents. Grey circles show individual data points in different oocytes. The chemical structure of the amino acids is shown on top of the bars and the error bars represent the SEM.

that the side-chain hydroxyl group is of much more importance than the aromatic function of the side chain for Na^+ binding/occlusion. Accordingly, mutations preserving some hydrogen bonding potential of the side chain, Y780C/H/S/T/Q, were less disturbing to Na^+ binding than removal of the hydroxyl group by Y780F. Furthermore, the experiments with unnatural substituents demonstrated that the introduction of tyrosine and phenylalanine derivatives with reduced cation–π interaction potential due to fluorination of the aromatic ring at the *m* position (*m*-*F*-Tyr or di-*m*-*F*-Phe) does not affect the interaction with external Na^+. The relatively small effects of fluorinating the phenylalanine at the *para* position (*p*-*F*-Phe) on the Q–V curve (small shift to the left, indicating a reduction of Na^+ apparent affinity) appear independent from the polarizability of the phenol ring and probably reflect steric hindrance effects of the fluorine at the position of the hydroxyl in tyrosine, as the Q–V shift is lost in oocytes expressing the double fluorinated di-*m*-*F*-Phe, relative to *p*-*F*-Phe. Taken together, these results indicate a rather minor importance of the cation–π interaction for the binding of Na^+.

Importantly, the non-aromatic substitution Y780Q increased the apparent Na^+ affinity twofold (corresponding to $\Delta\Delta G \sim -1.7$ kJ/mol). In contrast to all other mutations studied here, which reduced affinity by either removing the hydrogen bond (Y780A/F/L) or altering its optimal distance (Y780C/S/T/H), the Y780Q mutation introduces unique hydrogen bonding possibilities by the side-chain amide, which might form two hydrogen bonds, one with Q932 in M8 (similar to the WT tyrosine) and another with the side-chain oxygen of D817 in M6 (thus directly stabilizing the Na^+-binding side chain of D817 instead of through T816 by WT tyrosine). The glutamine substituent might also interact directly with the Na^+ ion at site III (although the side chain of the WT tyrosine appears to contribute only indirectly to Na^+ interaction, as discussed above). Considering that Y780Q has a largely reduced affinity for K^+ (as discussed later) and that the presence of external Na^+ increases the $K_{0.5}$ for K^+ by

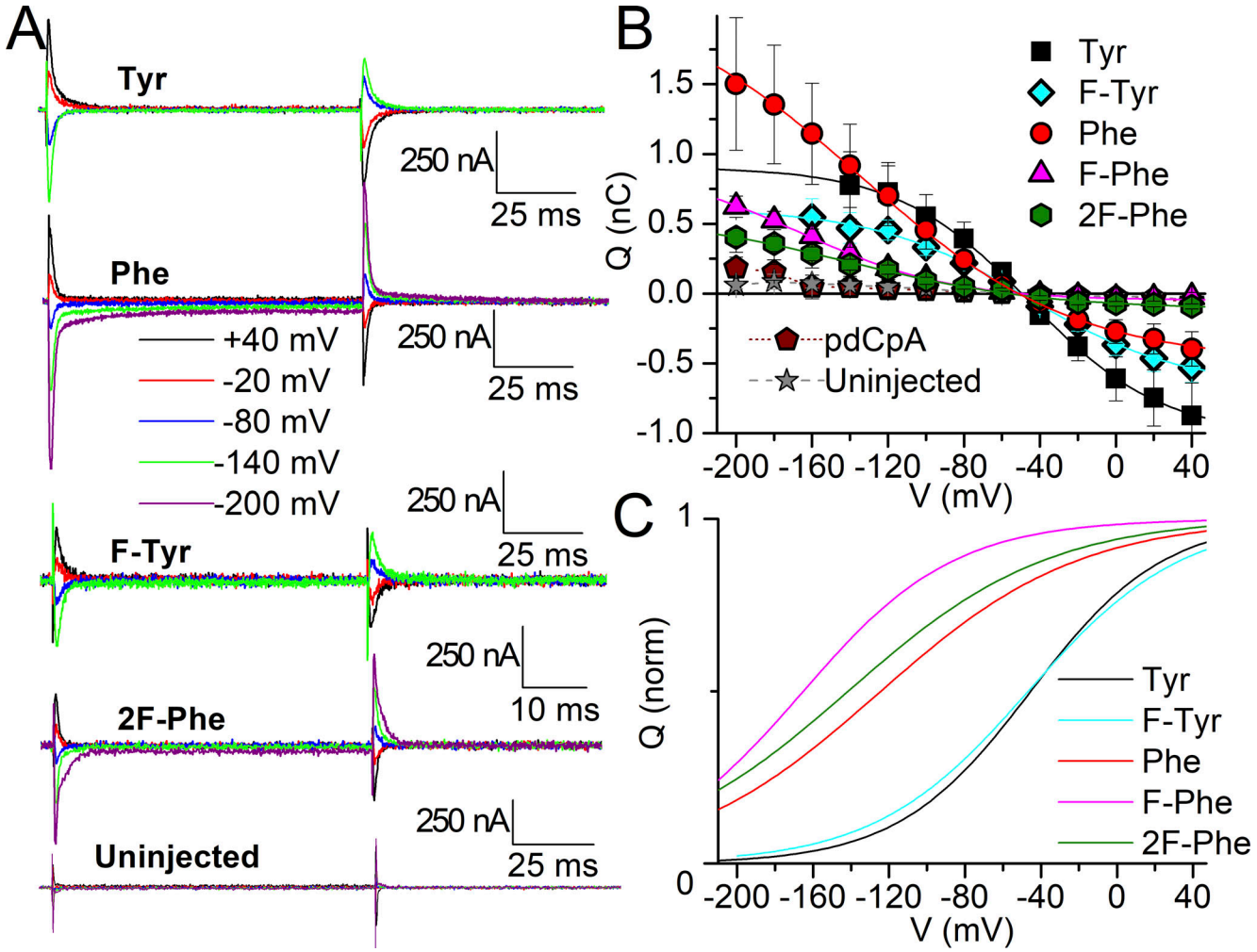

Figure 11. **Transient charge movement with unnatural amino acids at 780. (A)** Ouabain-sensitive traces elicited by applying pulses from −50 mV to the indicated voltages in oocytes either uninjected or injected using the non-sense suppression method with the indicated natural and unnatural amino acids. The current scale is identical for all traces. Time scale is different only for di-*m*-F-Phe (2F-Phe) for which pulses were 50 ms instead of 100 ms long. **(B)** Mean Q_{OFF}–V curve from experiments like those in A, number of experiments (four to nine) given with mean parameters from individual experiments in the text. The line plots are fits to Boltzmann distributions (Eq. 4) to the average data with parameters: $V_{1/2}$ = −45.6 mV, kT/z_qe = 35.0 mV, Q_{tot} = 1.91 nC for NSS-Tyr (Tyr); $V_{1/2}$ = −136 mV, kT/z_qe = 55.9 mV, Q_{tot} = 2.65 nC for NSS-Phe (Phe); $V_{1/2}$ = −46.7 mV, kT/z_qe = 40.3 mV, $V_{1/2}$ = −166 mV, kT/z_qe = 40 mV, Q_{tot} = 0.97 nC for *p*-F-Phe (F-Phe). Q_{tot} = 1.27 nC for *m*-F-Tyr (F-Tyr) $V_{1/2}$ = −141 mV, kT/z_qe = 52.0 mV, Q_{tot} = 0.68 nC for di-*m*-F-Phe (2F-Phe). Error bars represent the SEM. **(C)** Boltzmann fits to the average data, normalized to illustrate distinct voltage dependencies with parameters given in the text.

similar amounts (approximately fivefold) in both WT and Y780Q pumps, we infer that the affinity for Na^+ at sites I and II (where K^+ activates the enzyme and Na^+ and K^+ compete) is reduced in the mutant (otherwise, Na^+ should have reduced the affinity for K^+ more in the mutant than in the WT). Hence, the observed twofold increase in overall apparent affinity for Na^+ must specifically reflect an increase in Na^+ interaction affinity at site III (which exclusively interacts with Na^+), either by direct interaction with Na^+ or by a stronger hydrogen bond between the two amide groups to provide better coordination by Q932.

The tyrosine side chain has a large volume compared with most other amino acids with steric consequences. The differential effects of the substitutions with hydrophobic residues, Y780A/L/F, indicate an impact of the side-chain volume on Na^+ interaction. Alanine, for which the van der Waals volume is roughly half that of leucine and phenylalanine, reduced the apparent Na^+ affinity much more than the other hydrophobic substituents (~50-fold versus 12- and 16-fold for Y780L and Y780F, $\Delta\Delta G \sim +10$, +6, and +7 kJ/mol, respectively). The strong effect of removing the bulky side chain of Y780 is consistent with the crystal structure showing that it fills the interhelix space between M9, M5, and M6 (cf. the closeness of Y780 to P820 of M6, apparent on Fig. 1 C and D), the latter two helices contributing side chains participating in Na^+ coordination at all three sites (Kanai et al., 2013). Mutagenesis data for the corresponding tyrosine of the SERCA Ca^{2+} pump showed that glycine substitution resulted in complete uncoupling of Ca^{2+} transport from ATPase activity (but pump phosphorylation still required the presence of Ca^{2+}), whereas substitution with leucine allowed Ca^{2+} transport (Andersen, 1995; Andersen et al., 1997). Since Ca^{2+} binds at the analogous sites I and II, these results are consistent

with the importance of this tyrosine's side-chain volume to position the M6 aspartate of site I through hydrogen bonding of the juxtaposed threonine to the tyrosine. In keeping with this, most P2-ATPases, except PMCA, have a conserved tyrosine at the same M5 position (Fig. 1 E). Because PMCA binds only one Ca^{2+} (at site II), it does not need the hydrogen bond with the tyrosine hydroxyl group to fixate the unwound part of M6 for ion binding. However, the conservation of a large hydrophobic residue at the 780 position extends throughout the whole P-type ATPase family, as discussed below.

Various assays were used to examine mutational effects on apparent K^+ affinity with or without Na^+ present. All mutations studied, whether natural or fluorinated unnatural, weakened the K^+ interaction measured in the absence of Na^+ in electrophysiological experiments. The change in binding energy was $\Delta\Delta G \sim +5.5$ kJ/mol for Y780Q and Y780A, ~ +5 kJ/mol for Y780F and Y780S, ~ +4 kJ/mol for Y780T and Y780C, and ~ +2 kJ/mol for Y780L. These data suggest that the hydroxyl group of tyrosine is more critical than the aromatic function for K^+ interaction, just as was the case for Na^+ interaction. This conclusion is further strengthened by the rather small effect on K^+ affinity observed upon fluorination of the tyrosine (*m-F*-Tyr; $\Delta\Delta G \sim +1.7$ kJ/mol). Further consideration of the fluorination effects indicates that the characteristics of the chemical group at the *para* position of phenylalanine are a critical determinant of K^+ interaction. Compared with phenylalanine, a hydroxyl group (tyrosine) changes the binding energy corresponding to $\Delta\Delta G \sim -5.5$ kJ/mol, while a fluorine (*p*-F-Phe) changes the binding energy corresponding to $\Delta\Delta G \sim +4$ kJ/mol, which contrasts with the smaller effect of fluorination at the *para* position on the binding of Na^+ ($\Delta\Delta G \sim +2$ kJ/mol).

The effect of mutants Y780A/L/F/Q on K^+ interaction is not caused by a shift in the distribution of the phosphoenzyme intermediates E1P($3Na^+$) and E2P away from the K^+-binding E2P form in favor of E1P($3Na^+$) (Fig. 7 A). This indicates that the intrinsic affinity of the E2P form for K^+ is reduced in all the mutants. For Y780A/L/F, the reduction in apparent affinity for Na^+ was larger than the reduction in apparent affinity for K^+ measured without Na^+ present. Hence, there is a reduced competition by Na^+ for the same sites (I and II) when both ions are present, thereby explaining that the mutational effect on apparent K^+ affinity is minimal in the presence of Na^+. For Y780Q, the reduction in apparent affinity for K^+ in the presence of Na^+ is almost as large as in its absence, thus, the apparent affinity for Na^+ at sites I and II may be reduced, despite the increased affinity for Na^+ at site III discussed above. The sequential nature of external Na^+ release/rebinding (Castillo et al., 2011; Hilgemann, 1994; Holmgren et al., 2000; Moreno et al., 2020) hinders predicting by modeling and testing experimentally the exact increase and reduction of apparent affinity at each site.

The K^+ activation of current, as well as ATPase activity for which the apparent K^+ affinity was determined, occurs by K^+ binding to E2P sites facing the external side of the membrane. The two mutants Y780A/Q with the largest reduction in K^+ affinity also exhibited a marked increase in the apparent affinity for ATP in ATPase activity assay (Fig. 7 B), indicating an acceleration of the K^+ deoccluding E2($2K^+$) → E1 transition, which may be a consequence of destabilization of K^+ interaction in the occluded E2($2K^+$) form, similar to the effect of ATP binding to E2($2K^+$) (Holm et al., 2015; Post et al., 1972; Stanley et al., 2016). Both mutants also showed reduced dephosphorylation rate of E2P in the presence of Na^+ without K^+ (as seen by the lower rate of the slow exponential component in Fig. 7 A), suggesting that the affinity for Na^+ is reduced at one or both of the sites (I and II) where Na^+ can substitute for K^+ to activate E2P dephosphorylation, just as the K^+ affinity of these sites is reduced.

The two K^+ ions bound in the E2($2K^+$) form of the Na^+/K^+ pump occupy sites corresponding to sites I and II in the Na^+-bound E1 state with several identical ligand-binding residues (Kanai et al., 2013; Morth et al., 2007; Shinoda et al., 2009). However, because site III is selective for Na^+ and does not allow K^+ to bind (Ratheal et al., 2010), the side chain of Y780 cannot engage in a K^+–π interaction there, in agreement with the minor importance of the aromatic function for the binding of K^+ inferred from our experimental data. In the E2($2K^+$) form, the hydroxyl group of Y780 hydrogen binds directly to one of D817's side-chain oxygen atoms instead of interacting with T816 in M6, as seen for the Na^+ bound E1 state. The other side-chain oxygen of D817 interacts with a water molecule and serine S784, two contributors to K^+ coordination at site I in E2($2K^+$) (Fig. 1 D, water molecule shown as a red sphere, coordinated by both D817 and S784). This dependence of the hydrogen bond with D817 on the specific E1/E2 conformational state explains the critical role of Y780's hydroxyl group for K^+ interaction. Among the mutants Y780A/L/F/Q, the two with the smallest volume A and Q showed the largest reduction of K^+ affinity.

The experiments reported here were designed to test the functional effects of the mutations and not the structural effects causing reduced expression at the plasma membrane. With this in mind, we allowed the oocytes to express for the longest possible time to observe maximal signals with each mutant (or until substantial upregulation of pump expression had been achieved under ouabain-selective pressure in COS-1 cells). However, Y780D/E/Q/T/S/C/A all exhibited reduced expression levels (in some cases undetectable, i.e., Y780D/E), as indicated by less transient charge movement and K^+-induced pump currents. In contrast, Y780F/L/H all presented robust pump current and transient currents, which may indicate that residues with larger hydrophobic and/or cyclic side chains optimize protein folding and trafficking to the plasma membrane. Interestingly, the overwhelming majority of P-type ATPases (beyond the P2-ATPases, e.g., also P1-, P3-, and P4-ATPases as shown in Fig. 1 E) possess tyrosine at the equivalent position, while PMCA has phenylalanine. This high conservation among P-type ATPases may reflect the importance of the cyclic moiety at the position equivalent to Y780 for structural integrity. As demonstrated by the present results, the hydrogen bonds formed by the hydroxyl group add functional importance to the tyrosine in the Na^+/K^+ pump.

Notably, the substitutions equivalent to Y780C and Y780H in the neuronal α3-isoform of the Na^+/K^+ pump (Y768C and Y768H) cause the neurological disorder AHC. Compared with WT, these mutants exhibited increased passive steady-state current at negative voltages in the presence of Na^+ without K^+

(Fig. 8, A and F) and reduced apparent affinities for both transported ions (Fig. 8, B–E). Such enhanced "leak" currents have been observed in α3 mutants causing rapid-onset dystonia parkinsonism (a neurological disorder related to AHC; Isaksen et al., 2017) as well as in α1-subunit mutants that cause several disorders (recently reviewed by Biondo et al., 2021), including primary hyperaldosteronism (Azizan et al., 2013; Beuschlein et al., 2013; Meyer et al., 2017; Meyer et al., 2019) and hypomagnesemia with cognitive delay and seizures (Schlingmann et al., 2018). However, the inward leak in high external Na^+ is antagonized by external K^+ (which concomitantly activates pump current and inhibits the leak), and the net Na^+/K^+ pump current that was observed in both mutants at physiological K^+ is outward (Fig. 8 F), but near 0 for Y780H. Therefore, it seems unlikely that a gain-of-function passive inward current is the mechanism causing disease. Considering that a mouse model of rapid-onset dystonia parkinsonism has been generated by the perfusion of nanomolar concentrations of ouabain to inhibit α3 pumps (Calderon et al., 2011), and that the outward Na^+/K^+ pump current from α3 pumps has been shown to contribute to after-hyperpolarization potentials (important determinants of excitability following trains of pulses in pyramidal neurons; Gulledge et al., 2013), it is plausible that the loss of outward current in Y780C/H suffices to explain the pathologic increase in excitability without the need for an inward leak current.

In conclusion, by utilizing standard and non-sense suppression mutagenesis, we have demonstrated that the hydrogen-bond interactions of Y780 in M5 are essential for the binding of Na^+ and K^+ from both sides of the membrane, i.e., in the occluded states E1P($3Na^+$) and E2($2K^+$). A Na^+–π interaction with the phenol ring contributes minimally, if at all, to direct stabilization of Na^+ at the Na^+-exclusive site III. In addition to demonstrating the feasibility of non-sense suppression to perform atomic mutagenesis in slow-transport active transporters, our results further highlight the importance of the change of hydrogen bond network associated with the alteration between E1 and E2 conformational states as a determinant of the ion-binding affinities of the pump's major conformations. This hydrogen-bond–driven ion-selectivity switch is essential for Na^+/K^+ pump function.

Acknowledgments

Joseph A. Mindell served as editor.

We thank Nina Juste and Randi Scheel, Aarhus University, for expert technical assistance and Dylan J. Meyer for help with the patch experiments in Fig. 4.

This work was supported by grants MCB-1515434 and MCB-2003251 from the National Science Foundation and National Institutes of Health NINDS 1R03 NS116433-01 to P. Artigas, National Institute of Health grant NINDS 5R24 NS104617-04 to C.A. Ahern, and from the Lundbeck Foundation (grant R223-2016-595) and the Danish Council For Independent Research (grant 7016-00193B) to B. Vilsen.

The authors declare no competing financial intersts.

Author contributions: K. Spontarelli: conceptualization, data curation, formal analysis, validation, investigation, methodology, visualization, writing – original draft, review & editing. D.T. Infield: conceptualization, data curation, formal analysis, investigation, methodology, validation, visualization, writing – review & editing. H.N. Nielsen: data curation, formal analysis, investigation, methodology, supervision, validation, visualization, writing – review & editing. R. Holm: data curation, formal analysis, investigation, methodology, supervision, validation, visualization, writing – review & editing. V.C. Young: data curation, formal analysis, investigation, methodology, validation, visualization, writing – review & editing. J.D. Galpin: methodology, validation, writing – review & editing. C.A. Ahern: conceptualization, funding acquisition, methodology, project administration, resources, supervision, writing – review & editing. B. Vilsen: conceptualization, formal analysis, funding acquisition, investigation, project administration, resources, supervision, writing – original draft, review & editing. P. Artigas: conceptualization, data curation, formal analysis, funding acquisition, investigation, visualization, project administration, resources, supervision, writing – original draft, review & editing.

Submitted: 19 October 2021
Revised: 19 April 2022
Accepted: 16 May 2022

References

Ahern, C.A., A.L. Eastwood, D.A. Dougherty, and R. Horn. 2008. Electrostatic contributions of aromatic residues in the local anesthetic receptor of voltage-gated sodium channels. *Circ. Res.* 102:86–94. https://doi.org/10.1161/CIRCRESAHA.107.160663

Ahern, C.A., A.L. Eastwood, H.A. Lester, D.A. Dougherty, and R. Horn. 2006. A cation-pi interaction between extracellular TEA and an aromatic residue in potassium channels. *J. Gen. Physiol.* 128:649–657. https://doi.org/10.1085/jgp.200609654

Andersen, J.P. 1995. Functional consequences of alterations to amino acids at the M5S5 boundary of the $Ca^{(2+)}$-ATPase of sarcoplasmic reticulum. Mutation Tyr763→Gly uncouples ATP hydrolysis from Ca^{2+} transport. *J. Biol. Chem.* 270:908–914. https://doi.org/10.1074/jbc.270.2.908

Andersen, J.P., T. Sørensen, and B. Vilsen. 1997. Site-directed mutagenesis analysis of the role of the M5S5 sector of the sarcoplasmic reticulum $Ca^{(2+)}$-ATPase. *Ann. N. Y. Acad. Sci.* 834:333–338. https://doi.org/10.1111/j.1749-6632.1997.tb52264.x

Arguello, J.M., J. Whitis, M.C. Cheung, and J.B. Lingrel. 1999. Functional role of oxygen-containing residues in the fifth transmembrane segment of the Na,K-ATPase alpha subunit. *Arch. Biochem. Biophys.* 364:254–263. https://doi.org/10.1006/abbi.1999.1124

Azizan, E. A. B., H. Poulsen, P. Tuluc, J. Zhou, M.V. Clausen, A. Lieb, C. Maniero, S. Garg, E.G. Bochukova, W. Zhao, et al. 2013. Somatic mutations in ATP1A1 and CACNA1D underlie a common subtype of adrenal hypertension. *Nat. Genet.* 45:1055–1060. https://doi.org/10.1038/ng.2716

Baginski, E.S., P.P. Foa, and B. Zak. 1967. Microdetermination of inorganic phosphate, phospholipids, and total phosphate in biologic materials. *Clin. Chem.* 13:326–332

Beuschlein, F., S. Boulkroun, A. Osswald, T. Wieland, H.N. Nielsen, U.D. Lichtenauer, D. Penton, V.R. Schack, L. Amar, E. Fischer, et al. 2013. Somatic mutations in ATP1A1 and ATP2B3 lead to aldosterone-producing adenomas and secondary hypertension. *Nat. Genet.* 45:440–444.e1–2. https://doi.org/10.1038/ng.2550

Bezanilla, F., and C.A. Villalba-Galea. 2013. The gating charge should not be estimated by fitting a two-state model to a Q–V curve. *J. Gen. Physiol.* 142:575–578. https://doi.org/10.1085/jgp.201311056

Biondo, E.D., K. Spontarelli, G. Ababioh, L. Mendez, and P. Artigas. 2021. Diseases caused by mutations in the $Na^{(+)}/K^{(+)}$ pump alpha1 gene ATP1A1. *Am. J. Physiol. Cell Physiol.* 321:C394–C408. https://doi.org/10.1152/ajpcell.00059.2021

Calderon, D.P., R. Fremont, F. Kraenzlin, and K. Khodakhah. 2011. The neural substrates of rapid-onset Dystonia-Parkinsonism. *Nat. Neurosci.* 14: 357–365. https://doi.org/10.1038/nn.2753

Castillo, J.P., D. De Giorgis, D. Basilio, D.C. Gadsby, J.J.C. Rosenthal, R. Latorre, M. Holmgren, and F. Bezanilla. 2011. Energy landscape of the reactions governing the Na^+ deeply occluded state of the Na^+/K^+-ATPase in the giant axon of the humboldt squid. *Proc. Natl. Acad. Sci. USA*. 108: 20556–20561. https://doi.org/10.1073/pnas.1116439108

Chen, C., and H. Okayama. 1987. High-efficiency transformation of mammalian cells by plasmid DNA. *Mol. Cell. Biol.* 7:2745–2752. https://doi.org/10.1128/mcb.7.8.2745-2752.1987

Glynn, I.M. 1993. Annual review prize lecture. "All hands to the sodium pump". *J. Physiol.* 462:1–30. https://doi.org/10.1113/jphysiol.1993.sp019540

Gulledge, A.T., S. Dasari, K. Onoue, E.K. Stephens, J.M. Hasse, and D. Avesar. 2013. A sodium-pump-mediated afterhyperpolarization in pyramidal neurons. *J. Neurosci.* 33:13025–13041. https://doi.org/10.1523/JNEUROSCI.0220-13.2013

Hilgemann, D.W. 1994. Channel-like function of the Na, K pump probed at microsecond resolution in giant membrane patches. *Science*. 263: 1429–1432. https://doi.org/10.1126/science.8128223

Hohsaka, T., D. Kajihara, Y. Ashizuka, H. Murakami, and M. Sisido. 1999. Efficient incorporation of nonnatural amino acids with large aromatic groups into streptavidin in in vitro protein synthesizing systems. *J. Am. Chem. Soc.* 121:34–40. https://doi.org/10.1021/ja9813109

Holm, R., A.P. Einholm, J.P. Andersen, and B. Vilsen. 2015. Rescue of Na^+ affinity in aspartate 928 mutants of Na^+,K^+-ATPase by secondary mutation of glutamate 314. *J. Biol. Chem.* 290:9801–9811. https://doi.org/10.1074/jbc.M114.625509

Holm, R., J. Khandelwal, A.P. Einholm, J.P. Andersen, P. Artigas, and B. Vilsen. 2017. Arginine substitution of a cysteine in transmembrane helix M8 converts Na^+,K^+-ATPase to an electroneutral pump similar to H^+,K^+-ATPase. *Proc. Natl. Acad. Sci. USA* 114:316–321. https://doi.org/10.1073/pnas.1617951114

Holm, R., M.S. Toustrup-Jensen, A.P. Einholm, V.R. Schack, J.P. Andersen, and B. Vilsen. 2016. Neurological disease mutations of α3 Na^+,K^+-ATPase: Structural and functional perspectives and rescue of compromised function. *Biochim. Biophys. Acta*. 1857:1807–1828. https://doi.org/10.1016/j.bbabio.2016.08.009

Holmgren, M., and R.F. Rakowski. 1994. Pre-steady-state transient currents mediated by the Na/K pump in internally perfused *Xenopus* oocytes. *Biophys. J.* 66:912–922. https://doi.org/10.1016/s0006-3495(94)80867-7

Holmgren, M., and R.F. Rakowski. 2006. Charge translocation by the Na^+/K^+ pump under Na^+/Na^+ exchange conditions: Intracellular Na^+ dependence. *Biophys. J.* 90:1607–1616. https://doi.org/10.1529/biophysj.105.072942

Holmgren, M., J. Wagg, F. Bezanilla, R.F. Rakowski, P. De Weer, and D.C. Gadsby. 2000. Three distinct and sequential steps in the release of sodium ions by the Na^+/K^+-ATPase. *Nature*. 403:898–901. https://doi.org/10.1038/35002599

Infield, D.T., J.D. Lueck, J.D. Galpin, G.D. Galles, and C.A. Ahern. 2018. Orthogonality of pyrrolysine tRNA in the *Xenopus* oocyte. *Sci. Rep.* 8:5166. https://doi.org/10.1038/s41598-018-23201-z

Infield, D.T., A. Rasouli, G.D. Galles, C. Chipot, E. Tajkhorshid, and C.A. Ahern. 2021. Cation-pi interactions and their functional roles in membrane proteins. *J. Mol. Biol.* 433:167035. https://doi.org/10.1016/j.jmb.2021.167035

Isaksen, T.J., L. Kros, N. Vedovato, T.H. Holm, A. Vitenzon, D.C. Gadsby, K. Khodakhah, and K. Lykke-Hartmann. 2017. Hypothermia-induced dystonia and abnormal cerebellar activity in a mouse model with a single disease-mutation in the sodium-potassium pump. *PLoS Genet.* 13: e1006763. https://doi.org/10.1371/journal.pgen.1006763

Kanai, R., H. Ogawa, B. Vilsen, F. Cornelius, and C. Toyoshima. 2013. Crystal structure of a Na^+-bound Na^+,K^+-ATPase preceding the E1P state. *Nature*. 502:201–206. https://doi.org/10.1038/nature12578

Leisle, L., R. Chadda, J.D. Lueck, D.T. Infield, J.D. Galpin, V. Krishnamani, J.L. Robertson, and C.A. Ahern. 2016. Cellular encoding of Cy dyes for single-molecule imaging. *Elife*. 5:e19088. https://doi.org/10.7554/eLife.19088

Leisle, L., F. Valiyaveetil, R.A. Mehl, and C.A. Ahern. 2015. Incorporation of non-canonical amino acids. *Adv. Exp. Med. Biol.* 869:119–151. https://doi.org/10.1007/978-1-4939-2845-3_7

Meier, S., N.N. Tavraz, K.L. Durr, and T. Friedrich. 2010. Hyperpolarization-activated inward leakage currents caused by deletion or mutation of carboxy-terminal tyrosines of the Na^+/K^+-ATPase {α} subunit. *J. Gen. Physiol.* 135:115–134. https://doi.org/10.1085/jgp.200910301

Meyer, D.J., S. Bijlani, M. de Sautu, K. Spontarelli, V.C. Young, C. Gatto, and P. Artigas. 2020. FXYD protein isoforms differentially modulate human Na/K pump function. *J. Gen. Physiol.* 152:e202012660. https://doi.org/10.1085/jgp.202012660

Meyer, D.J., C. Gatto, and P. Artigas. 2017. On the effect of hyperaldosteronism-inducing mutations in Na/K pumps. *J. Gen. Physiol.* 149:1009–1028. https://doi.org/10.1085/jgp.201711827

Meyer, D.J., C. Gatto, and P. Artigas. 2019. Na/K pump mutations associated with primary hyperaldosteronism cause loss of function. *Biochemistry*. 58:1774–1785. https://doi.org/10.1021/acs.biochem.9b00051

Moreno, C., S. Yano, F. Bezanilla, R. Latorre, and M. Holmgren. 2020. Transient electrical currents mediated by the $Na^{(+)}/K^{(+)}$-ATPase: A tour from basic biophysics to human diseases. *Biophys. J.* 119:236–242. https://doi.org/10.1016/j.bpj.2020.06.006

Morth, J.P., B.P. Pedersen, M.S. Toustrup-Jensen, T.L.M. Sørensen, J. Petersen, J.P. Andersen, B. Vilsen, and P. Nissen. 2007. Crystal structure of the sodium-potassium pump. *Nature*. 450:1043–1049. https://doi.org/10.1038/nature06419

Nielsen, H.N., K. Spontarelli, R. Holm, J.P. Andersen, A.P. Einholm, P. Artigas, and B. Vilsen. 2019. Distinct effects of Q925 mutation on intracellular and extracellular $Na^{(+)}$ and $K^{(+)}$ binding to the $Na^{(+)}$, $K^{(+)}$-ATPase. *Sci. Rep.* 9:13344. https://doi.org/10.1038/s41598-019-50009-2

Panagiotakaki, E., E. De Grandis, M. Stagnaro, E.L. Heinzen, C. Fons, S. Sisodiya, B. de Vries, C. Goubau, S. Weckhuysen, D. Kemlink, et al. 2015. Clinical profile of patients with ATP1A3 mutations in Alternating Hemiplegia of Childhood-a study of 155 patients. *Orphanet J. Rare Dis.* 10: 123. https://doi.org/10.1186/s13023-015-0335-5

Pedersen, P.A., J.M. Nielsen, J.H. Rasmussen, and P.L. Jorgensen. 1998. Contribution to Tl^+, K^+, and Na^+ binding of Asn776, Ser775, Thr774, Thr772, and Tyr771 in cytoplasmic part of fifth transmembrane segment in alpha-subunit of renal Na,K-ATPase. *Biochemistry*. 37:17818–17827. https://doi.org/10.1021/bi981898w

Pless, S.A., J.D. Galpin, A. Frankel, and C.A. Ahern. 2011a. Molecular basis for class Ib anti-arrhythmic inhibition of cardiac sodium channels. *Nat. Commun.* 2:351. https://doi.org/10.1038/ncomms1351

Pless, S.A., J.D. Galpin, A.P. Niciforovic, and C.A. Ahern. 2011b. Contributions of counter-charge in a potassium channel voltage-sensor domain. *Nat. Chem. Biol.* 7:617–623. https://doi.org/10.1038/nchembio.622

Post, R.L., C. Hegyvary, and S. Kume. 1972. Activation by adenosine triphosphate in the phosphorylation kinetics of sodium and potassium ion transport adenosine triphosphatase. *J. Biol. Chem.* 247: 6530–6540

Ratheal, I.M., G.K. Virgin, H. Yu, B. Roux, C. Gatto, and P. Artigas. 2010. Selectivity of externally facing ion-binding sites in the Na/K pump to alkali metals and organic cations. *Proc. Natl. Acad. Sci. USA*. 107: 18718–18723. https://doi.org/10.1073/pnas.1004214107

Robertson, S.A., J.A. Ellman, and P.G. Schultz. 1991. A general and efficient route for chemical aminoacylation of transfer-Rnas. *J. Am. Chem. Soc.* 113:2722–2729. https://doi.org/10.1021/ja00007a055

Roux, B. 2005. Ion conduction and selectivity in $K^{(+)}$ channels. *Annu. Rev. Biophys. Biomol. Struct.* 34:153–171. https://doi.org/10.1146/annurev.biophys.34.040204.144655

Santarelli, V.P., A.L. Eastwood, D.A. Dougherty, R. Horn, and C.A. Ahern. 2007. A cation-pi interaction discriminates among sodium channels that are either sensitive or resistant to tetrodotoxin block. *J. Biol. Chem.* 282:8044–8051. https://doi.org/10.1074/jbc.M611334200

Schlingmann, K.P., S. Bandulik, C. Mammen, M. Tarailo-Graovac, R. Holm, M. Baumann, J. Konig, J.J.Y. Lee, B. Drogemoller, K. Imminger, et al. 2018. Germline de novo mutations in ATP1A1 cause renal hypomagnesemia, Refractory seizures, and intellectual disability. *Am. J. Human Gen.* 103:808–816. https://doi.org/10.1016/j.ajhg.2018.10.004

Sen, A.K., and R.L. Post. 1964. Stoichiometry and localization of adenosine triphosphate-dependent sodium and potassium transport in the erythrocyte. *J. Biol. Chem.* 239:345–352

Shinoda, T., H. Ogawa, F. Cornelius, and C. Toyoshima. 2009. Crystal structure of the sodium-potassium pump at 2.4 A resolution. *Nature*. 459:446–450. https://doi.org/10.1038/nature07939

Stanley, C.M., D.G. Gagnon, A. Bernal, D.J. Meyer, J.J. Rosenthal, and P. Artigas. 2015. Importance of the voltage dependence of cardiac Na/K ATPase isozymes. *Biophys. J.* 109:1852–1862. https://doi.org/10.1016/j.bpj.2015.09.015

Stanley, K.S., D.J. Meyer, C. Gatto, and P. Artigas. 2016. Intracellular requirements for passive proton transport through the $Na^{(+)}$,$K^{(+)}$-ATPase. *Biophys. J.* 111:2430–2439. https://doi.org/10.1016/j.bpj.2016.09.042

Tian, Y., M. Aursnes, T.V. Hansen, J.E. Tungen, J.D. Galpin, L. Leisle, C.A. Ahern, R. Xu, S.H. Heinemann, and T. Hoshi. 2016. Atomic determinants of BK channel activation by polyunsaturated fatty acids. *Proc. Natl. Acad. Sci. USA.* 113:13905–13910. https://doi.org/10.1073/pnas.1615562113

Vedovato, N., and D.C. Gadsby. 2010. The two C-terminal tyrosines stabilize occluded Na/K pump conformations containing Na or K ions. *J. Gen. Physiol.* 136:63–82. https://doi.org/10.1085/jgp.201010407

Vilsen, B. 1995. Mutant Glu781→Ala of the rat kidney Na^+,K^+-ATPase displays low cation affinity and catalyzes ATP hydrolysis at a high rate in the absence of potassium ions. *Biochemistry.* 34:1455–1463. https://doi.org/10.1021/bi00004a041

Yaragatupalli, S., J.F. Olivera, C. Gatto, and P. Artigas. 2009. Altered Na^+ transport after an intracellular alpha-subunit deletion reveals strict external sequential release of Na^+ from the Na/K pump. *Proc. Natl. Acad. Sci. USA.* 106:15507–15512. https://doi.org/10.1073/pnas.0903752106

Zhong, W., J.P. Gallivan, Y. Zhang, L. Li, H.A. Lester, and D.A. Dougherty. 1998. From ab initio quantum mechanics to molecular neurobiology: A cation-pi binding site in the nicotinic receptor. *Proc. Natl. Acad. Sci. USA.* 95:12088–12093. https://doi.org/10.1073/pnas.95.21.12088